

Chandra X-ray Sources in the LALA Cetus Field¹

J. X. Wang², Z. Y. Zheng², S. Malhotra³, S. L. Finkelstein⁴, J. E. Rhoads³, C. A. Norman⁵,
T. M. Heckman⁵

ABSTRACT

The 174 ks *Chandra* Advanced CCD Imaging Spectrometer exposure of the Large Area Lyman Alpha Survey (LALA) Cetus field is the second of the two deep *Chandra* images on LALA fields. In this paper we present the *Chandra* X-ray sources detected in the Cetus field, along with an analysis of X-ray source counts, stacked X-ray spectrum, and optical identifications. A total of 188 X-ray sources were detected: 174 in the 0.5 – 7.0 keV band, 154 in the 0.5 – 2.0 keV band, and 113 in the 2.0 – 7.0 keV band. The X-ray source counts were derived and compared with LALA Boötes field (172 ks exposure). Interestingly, we find consistent hard band X-ray source density, but $36\pm 12\%$ higher soft band X-ray source density in Cetus field. The weighted stacked spectrum of the detected X-ray sources can be fitted by a powerlaw with photon index $\Gamma = 1.55$. Based on the weighted stacked spectrum, we find that the resolved fraction of the X-ray background drops from $72\pm 1\%$ at 0.5 – 1.0 keV to $63\pm 4\%$ at 6.0 – 8.0 keV. The unresolved spectrum can be fitted by a powerlaw over the range 0.5 – 7 keV, with a photon index $\Gamma = 1.22$. We also present optical counterparts for 154 of the X-ray sources, down to a limiting magnitude of $r' = 25.9$ (Vega), using a deep r' band image obtained with the MMT.

Subject headings: catalogs — galaxies: active — galaxies: high-redshift — X-rays: diffuse background — X-rays: galaxies

¹Optical Observations reported here were obtained at the MMT Observatory, a joint facility of the University of Arizona and the Smithsonian Institution.

²Center for Astrophysics, University of Science and Technology of China, Hefei, Anhui 230026, P. R. China; jxw@ustc.edu.cn.

³School of Earth and Space Exploration, Arizona State University, Tempe, AZ 85287

⁴Department of Physics, Arizona State University, Tempe, AZ 85287

⁵Department of Physics and Astronomy, Johns Hopkins University, Baltimore, MD, 21218

1. Introduction

The launch of the *Chandra X-Ray Observatory* in 1999 has opened a new era of X-ray astronomy, thanks to its superb spatial resolution and sensitivity (Weisskopf et al. 2002). In recent years, many deep *Chandra* images of the extragalactic sky have been obtained, including the 2 Ms *Chandra* Deep Field North (CDF-N, e.g., Brandt et al. 2001; Alexander et al. 2003), 1 Ms *Chandra* Deep Field South (CDF-S, Giacconi et al. 2002; Rosati et al. 2002), and many others at moderate depths (Stern et al. 2002; Yang et al. 2003; Mushotzky et al. 2000; Manners et al. 2003; Wang et al. 2004a, 2004b; see Brandt & Hasinger 2005 for a full list of deep extragalactic *Chandra* exposures). The European Space Agency’s X-ray Multi-Mirror Mission-Newton (XMM-Newton; Jansen et al. 2001) has provided a comparable number of surveys (again listed by Brandt & Hasinger 2005). These deep images alone resolved the majority 0.1 – 10 keV X-ray background. Worsley et al (2005) present a detailed study of the fraction of resolved X-ray background as a function of energy. Together with multi-band follow-up observations, these deep images provide large samples of X-ray sources, and enable studies of the formation and evolution of galaxies, clusters and groups of galaxies, large-scale structures, and super massive black holes (SMBH).

In this paper we present a new deep (174 ks) *Chandra* ACIS exposure of the Large Area Lyman Alpha (LALA; Rhoads et al. 2000) survey’s Cetus field. This is the second of two deep *Chandra* images of LALA fields. The previous one is an 172 ks ACIS exposure of LALA Boötes field (Malhotra et al. 2003, Wang et al. 2004a). The X-ray image presented here was originally obtained to investigate the X-ray properties of the LALA detected high redshift Ly α emitters (Wang et al., 2004b). In this paper we present a full catalog of the detected X-ray sources, along with an analysis of the resolved X-ray background, and optical identifications using deep broad band images obtained with the 6.5m MMT + Megacam on Mt. Hopkins, Arizona.

2. X-ray Observations and Data Reduction

A total of 176 ks of *Chandra* ACIS exposure on the LALA Cetus field was obtained in very faint (VFAINT) mode, composed of two individual observations. The first observation, with 160.4 ks exposure, was taken on UT 2002 June 13–14 (*Chandra* Obs ID 4129). The second observation, with 15.4 ks exposure, was taken one day later (UT 2002 June 15, Obs ID 4402). All four ACIS-I chips and the ACIS-S2, ACIS-S3 chips were used, with the telescope aimpoint centered on the ACIS-I3 chip for each exposure. The aimpoints of both exposures were R.A. = 02:04:44.081, decl. = –05:05:17.36 (J2000.0). Due to their large off-axis angle during the observations, the ACIS-S chips have poorer spatial resolution and

effective area than the ACIS-I chips. We have therefore chosen to ignore the ACIS-S chip data in this work. We reduced the data using the packages CIAO 3.3 and CALDB 3.2.2 (see <http://asc.harvard.edu/ciao>). The level 1 data were reprocessed to clean the ACIS particle background for the VFAINT mode observations, and filtered to include only the standard event grades 0, 2, 3, 4, and 6. All bad pixels and columns were also removed. We excluded high background time intervals from level 2 files, leaving a net exposure time of 174 ks. We extracted three images from the combined event file: a soft image (0.5 – 2.0 keV), a hard image (2.0 – 7.0 keV) and a total image (0.5 – 7.0 keV). We cut the hard and total bands at 7 keV, because the effective area of *Chandra* decreases and the particle/cosmic ray background rises above this energy, resulting in very inefficient detection of sky and source photons.

3. Source Detection and Catalog

We ran WAVDETECT (Freeman et al. 2002) on the extracted X-ray images using a probability threshold of 1×10^{-7} (corresponding to 0.5 false sources expected per image). We used wavelet scales of 1, $\sqrt{2}$, 2, $2\sqrt{2}$, 4, $4\sqrt{2}$, 8, $8\sqrt{2}$, 16, $16\sqrt{2}$, and 32 pixels (where 1 pixel = 0.492"). A total of 188 X-ray sources were detected: 174 in the total band (0.5 – 7.0 keV), 154 in the soft band (0.5 – 2.0 keV), and 113 in the hard band (2.0 – 7.0 keV)¹. The catalog of the detected sources is presented in Table 1.

The source ID, IAU name, right ascension and declination are presented in Table 1. The IAU name for the sources is CXOLALA2 JHHMMSS.s+DDMMSS. Whenever available, source coordinates derived in the soft band image, which has the best spatial resolution among the three bands, are presented. For sources not detected in the soft band, total (with a higher priority) or hard band positions are used as substitutions. Column 5 in table 1 gives the 3σ uncertainties of the centroid positions directly given by WAVDETECT. We perform circular aperture photometry to measure the net counts in each band for all the 188 detected sources (Column 6-8). For each source, we defined a source region which is a circle centered at the source position (column 3 and 4 in Table 1), with radius R_s set to the 95% encircled-energy radius of *Chandra* ACIS PSF at 1.5 keV. R_s varies in the range of 2" to 15" from the center to the edge of the field. Source photons were then extracted from the circles, and the local background was extracted from an annulus with outer radius of $2.4 \times R_s$ and inner radius of $1.2 \times R_s$, after masking out nearby sources. The aperture correction

¹Changing the WAVDETECT probability threshold to 1×10^{-6} increases the total number of detected X-ray sources to 213. However, this would increase the expected number of false detections to ~ 5 per image, and we prefer to publish a conservative catalog with high reliability.

($\times 1/0.95$) was applied to the source counts. While this correction is based on the PSF at 1.5 keV, and could be refined to account for the variation of PSF with photon energy and the spectral slopes of sources, such higher order corrections would have a negligible impact on our final count rates. The derived net counts and 1σ Poisson uncertainties² are given for each source in each band.

In column 9 we mark the sources with “T”, “S” and “H” for detection in total, soft and hard band respectively. Multiple letters are used for sources detected in more than one band. In column 10 we present the hardness ratios. Here we calculate the hardness ratios with a Bayesian approach which models the detected counts as a Poisson distribution and can give reliable errorbars for both low and high count sources (van Dyk et al. 2004; Park et al. 2006). The hardness ratios versus 0.5 – 10.0 keV band X-ray fluxes for the detected X-ray sources are plotted in Fig. 1. Assuming a power-law spectrum with the Galactic HI column density ($2.2 \times 10^{20} \text{ cm}^{-2}$), the observed hardness ratio can be converted to the photon index Γ of the spectrum, which is also presented in the figure. An increasing proportion of hard sources is seen at the fainter flux levels (an effect seen also in earlier surveys). Most of these are believed to be obscured AGNs.

In column 11-13 we present X-ray fluxes (Galactic absorption corrected, $N_H = 2.2 \times 10^{20} \text{ cm}^{-2}$, Dickey & Lockman 1990) in three bands. We assumed a power-law spectrum, absorbed by the Galactic column density, to calculate the conversion factors from net counts to X-ray fluxes. We used a photon index of $\Gamma = 1.4$, as previously used by Giacconi et al. (2002), Stern et al. (2002) and Wang et al. (2004a). Net count rates were calculated by dividing the net counts in column 6-8 by the effective exposure time at each source position in each band. We then converted these into X-ray fluxes in 0.5 – 10.0 keV, 0.5 – 2.0 keV, and 2.0 – 10.0 keV bands respectively. The conversion factors adopted are $1.35 \times 10^{-11} \text{ ergs cm}^{-2} \text{ count}^{-1}$ for the total band; $5.66 \times 10^{-12} \text{ ergs cm}^{-2} \text{ count}^{-1}$ for the soft band; and $2.65 \times 10^{-11} \text{ ergs cm}^{-2} \text{ count}^{-1}$ for the hard band. As we have pointed in Wang et al. (2004a), the total band flux differs from the sum of the soft and hard band fluxes if the actual photon index differs from 1.4. In Fig. 2 we plot the conversion factors required assuming a power-law spectrum with different photon index Γ . It is obvious in the figure that the conversion factors in hard and total band are quite sensitive to the assumed Γ . We thus need to be cautious while using the fluxes obtained assuming a constant Γ .

²We use Bayesian method to get the net counts and 1σ Poisson uncertainties (e.g., Kraft et al, 1991).

4. X-ray source counts

Since *Chandra* ACIS does not have uniform sensitivity across the field of view, our survey’s sky coverage is a function of source flux. (That is, brighter sources can be detected with larger sky area.) To calculate the sky coverage, we first determine the formal signal to noise ratio,

$$S/N = (NET_{cts})/\sqrt{(NET_{cts} + BG_{cts})}, \quad (1)$$

that is required to ensure a high confidence detection in WAVDETECT, as a function of off-axis angle in the field. To do this, we present in figure 3 the soft, hard, and total band S/N ratio versus off-axis angle θ for the X-ray sources detected in each band. In each panel, nondetections are displayed with different symbols. (“Nondetections” here means sources not detected in that band, along with additional sources detected in that band but using a less significant WAVDETECT probability threshold³)

It’s clear from the figure that the minimum S/N required to ensure a high confidence detection increases with the off-axis angle. Thus, instead of using a constant S/N limit across the field, we use a variable S/N limit dependent on the off-axis angle. Three dashed lines ($S/N = A + B \times \theta$ respectively) are shown in fig. 3, with the parameters A and B chosen by visual inspection to include maximum number of detected sources in each band but at most one nondetection above the lines. Although there are detected sources below the threshold lines, they are mixed up with nondetections, i.e., the detection is incomplete below the lines. In this paper, we use only these sources with $S/N > A + B \times \theta$ to calculate LogN-LogS⁴. We then use our derived cutoff as a function of angle to determine the sky coverages as a function of flux. The resulting area-flux curves are shown in Fig. 4, and the resulting log N -log S relations for both soft and hard bands in Fig. 5. We measured the slope of the log N -log S with a maximum likelihood power law fit in each band. For the 0.5 – 2.0 keV band we find

$$N(> S) = 542_{-18}^{+18} \times \left(\frac{S}{2. \times 10^{-15} \text{ ergs cm}^{-2} \text{ s}^{-1}} \right)^{-0.806_{-0.024}^{+0.024}} \quad (2)$$

and for the 2.0 – 10.0 keV band

$$N(> S) = 1577_{-53}^{+52} \times \left(\frac{S}{2. \times 10^{-15} \text{ ergs cm}^{-2} \text{ s}^{-1}} \right)^{-1.033_{-0.035}^{+0.036}} \quad (3)$$

³We use different probability threshold of WAVDETECT, 1×10^{-6} , 1×10^{-5} and 1×10^{-4} , to extract additional sources.

⁴A = 2.24, 2.24, 2.7 and B = 0.13, 0.19 0.10 for the soft, hard and tot band respectively.

The error bars here are 1σ errors derived from $\Delta\chi_{\nu=2}^2 = 2.30$ (e.g., Lampton et al. 1976).

For comparison, we re-reduced the 172 ks Chandra exposure on LALA Boötes field following the same procedures described above, and obtained the source counts. This minimized the possible bias due to the difference between calibrations and data reductions. In the Boötes field, we detected 167 sources in the 0.5 – 7.0 keV band, 139 in the 0.5 – 2.0 keV band, and 118 in the 2.0 – 7.0 keV band. Note the numbers are slightly different from those published in Wang et al (2004a) due to the different version of calibration files and source detections procedures. Comparing with the Boötes field, in the Cetus field we detect fewer sources in the hard band (113 vs 118), but more sources in the soft band (154 vs 139). Since the source numbers in the soft and hard band are not independent quantities, the soft band over density in the Cetus field is much more significant than it appears in the number ratio 154 vs 139. A rough estimation can be made based the facts that soft band detected sources outnumbers hard band ones by 41 in the Cetus field and 21 in the Boötes field. This (41 vs 21) corresponds to a 2.8σ excess in the Cetus field. Note such calculation is only valid if all of the hard band detected sources are also detected in the soft band. For our case in this paper, the accurate significant level should be close to 2.8σ since most (82%) of the hard band detected sources in both fields show up in the soft band.

Note the actual source density depends on the sky coverage and also the Galactic absorption which affects the observed soft band count rates. We point out the soft band excess in the Cetus field can not be attributed to these effects, since it has even slightly smaller sky coverage and larger Galactic absorption comparing with the Boötes field. In the plot of LogN-LogS (see Fig. 5) where these effects have been corrected, it is also clear that while two fields are consistent in the hard band source density, the Cetus field has $36\pm 12\%$ higher source density (substantially above the Poisson noise) in the soft band at 2.0×10^{-15} erg cm^{-2} s^{-1} . Following Wang et al. (2004a), we also plot LogN-LogS from different fields for comparison (CDF-N, Brandt et al. 2001; CDF-S, Rosati et al. 2002; Lynx, Stern et al. 2002). We note that the soft band excess in the Cetus field is also obvious ($36\pm 12\%$) comparing with the mean of the five fields.

5. The resolved X-ray background and the stacked X-ray spectrum

What fraction of the hard X-ray background is resolved by our deep 174 ks *Chandra* imaging? We try to find the answer with two different approaches. We first calculate the fraction from the LogN-LogS. In the flux range of $1.15 - 100 \times 10^{-15}$ ergs cm^{-2} s^{-1} , the integrated hard X-ray flux density in the 2.0 – 10.0 keV band is 1.28×10^{-11} ergs cm^{-2} s^{-1} deg^{-2} . This corresponds to 57% of the 2. – 10.0 keV band X-ray background (De Luca &

Molendi 2004). Note that there is no source brighter than 1.0×10^{-13} ergs cm^{-2} s^{-1} in the Cetus field. By combining with the wide area *ASCA* Large Sky Survey (with sky coverage of ~ 7 deg², Ueda et al. 1999) which resolves 0.46×10^{-11} ergs cm^{-2} s^{-1} deg⁻² down to a flux limit of 1.0×10^{-13} ergs cm^{-2} s^{-1} in the 2 – 10 keV band, we obtained a higher fraction of 77.6%.

Recently attempts have been made to measure the resolved fraction of XRB as a function of energy in deep Chandra/XMM surveys. By stacking X-ray sources in Chandra Deep Fields and XMM Lockman Hole in narrower photometric bands, Worsley et al. (2004; 2005) have shown that the resolved fraction of XRB drops from 80-100% at < 2 keV to $\sim 50\%$ at above 8 keV. The fraction as a function of energy can be used to estimate the spectral shape of the unresolved XRB and the population of sources contributing it. In this paper we adopt a different approach to estimate the intensity spectrum of the resolved XRB in the LALA Cetus field. The resolved XRB intensity spectrum was obtained by summing the unfolded spectrum for each detected X-ray source divided by its sky coverage. In §4 we have obtained the soft, hard and total band sky coverage for each source. We use the largest of these three areas for each source when constructing our composite spectrum. We exclude sources with sky coverage < 0.003 degree², to avoid large uncertainties due to small sky coverage. The unfolded spectra were obtained assuming a powerlaw with $\Gamma = 1.4$ absorbed by Galactic hydrogen column density. Adopting slightly different Γ as 1.2 or 1.6 does not change our results below. The stacked X-ray spectral intensity is presented in Fig. 6, which is best-fitted by a powerlaw with photon index $\Gamma = 1.55 \pm 0.02$ and normalization of 8.23 ± 0.07 photons $\text{cm}^{-2}\text{s}^{-1}\text{sr}^{-1}\text{keV}^{-1}$.

We adopt the XRB model spectrum used by Worsley et al. (2005), which is a power-law with a spectral slope of $\Gamma = 1.41$ in the 1 – 8 keV band (De Luca & Molendi 2004). Below 1 keV, we use the measurement at 0.25 keV from Roberts & Warwick (2001), which yields a spectral slope of $\Gamma = 1.6$. We thus see that the resolved fraction of the X-ray background in Cetus field can be modeled as $0.72 \times E^{-0.14}$, decreasing from 72% at 1 keV to 54% at 8 keV. There are very large uncertainties above 8 keV, due to the limited photons in that band. We did not attempt to make corrections for very bright sources which are absent in such a small field. We also plot the resolved fraction of XRB in CDF-N and CDF-S obtained by Worsley et al. (2005). In the 0.5-1 keV band, the resolved fraction in the Cetus field is comparable with those of CDFS. This is mainly due to the higher source density in the Cetus field as we found in §4. The fraction decreases from 1 keV to 8 keV and is obviously smaller than CDFs, because of the less exposure time in the Cetus field. We note that to avoid the bias caused by cosmic variance, accurate measurements of the resolved and unresolved spectra require combining deep surveys with shallow wide area surveys.

6. Optical Identifications

Deep broadband images on LALA Cetus field were obtained in four Sloan Digital Sky Survey (SDSS) filters (g' , r' , i' , and z') using the Megacam instrument (McLeod et al. 1998) at the MMT. The total exposure time in the g' , r' , i' , and z' 4.33, 3.50, 4.78 and 5.33 hours respectively. The details of the observations and data reduction have been presented in Finkelstein et al. (2007), who used the deep broadband images to study the ages and masses of Ly α emitters at $z \sim 4.5$. The 5σ limiting magnitudes (2.32" diameter aperture) obtained are 26.38, 25.64, 25.13 and 24.1 (Vega) respectively in four bands.

We use the MMT r' band to identify our X-ray sources. We find the astrometry of the X-ray image and the MMT images are well matched, with an average shift less than 0.1". We use circles with radius equals the root sum square of the 3σ positional uncertainties from WAVDETECT for X-ray sources (see table 1) and 1". Here 1" stands for the uncertainty in the absolute X-ray astrometry. Optical counterparts in r' band are found for 158 X-ray sources. We find two possible counterparts each for three of these X-ray sources. In table 1, we only present the one which is closer to the center of the search circle. Two of the X-ray sources are located outside the MMT image. There are also 8 sources which are too close to nearby bright sources, making it impossible to identify them in the optical band image and to provide reliable upper limits to their r' band magnitudes. For the remaining 20 X-ray sources without r' band counterparts, we tabulate the 5σ r' band upper limits, i.e. 25.86⁵).

In column 14-16 in Table 1 we present the offsets of the detected optical counterparts from the X-ray source positions ($\Delta\alpha = \text{RA}_R - \text{RA}_X$, $\Delta\delta = \text{Dec}_R - \text{Dec}_X$), and the r' band AUTO magnitudes from SExtractor (Kron-like elliptical aperture magnitudes, Bertin & Arnouts 1996) together with their 1σ uncertainties⁶. For sources which are not detected in r' band, 5σ upper limits of the magnitudes are given when available.

Among the 20 X-ray sources without r' band counterparts, four have counterparts in the g' band MMT image. The remaining 16 sources, which are not detected either in the g' or r' band, are possible candidates for $z > 5$ quasars, since such sources would be invisible in the g' or r' band because of the absorption from the Lyman transitions of hydrogen along our line of sight. However, 8 of these 16 sources have X-ray hardness ratio $HR > 0.0$, indicating strong X-ray obscuration. This suggests that they are X-ray obscured AGNs at

⁵This is the mean Vega magnitude of SExtractor detected sources with signal to noise ratio around 5, and thus differs slightly from the 5σ limiting magnitude in a 2.32" diameter aperture that is reported above.

⁶The uncertainties of the magnitudes are direct output from SExtractor, without including the uncertainty of the r' band zeropoint.

low to at most intermediate redshift, because even heavily obscured AGNs at $z > 5$ would appear soft in *Chandra* images due to redshifting of the X-ray spectrum (Wang et al. 2004c). This reduce the number of candidate $z > 5$ quasars to 8. A program to obtain the optical spectra of these X-ray sources using the Inamori-Magellan Areal Camera and Spectrograph (IMACS) on the Magellan 6.5m telescopes is under way.

7. Conclusions

We present X-ray sources detected in 174 ks of *Chandra* ACIS integration on the LALA Cetus field. A total of 188 X-ray sources were detected: 174 in the total band (0.5 – 7.0 keV), 154 in the soft band (0.5 – 2.0 keV), and 113 in the hard band (2.0 – 7.0 keV). The detection near the aimpoint is down to a flux limit of 2.5×10^{-16} ergs cm^{-2} s^{-1} in the soft (0.5 – 2.0 keV) band, and 1.15×10^{-15} ergs cm^{-2} s^{-1} in the hard (2.0 – 10.0 keV) band. Comparing with LALA Boötes field, we obtain comparable X-ray source density in the hard band, but $36 \pm 12\%$ higher source density in the soft band. We study the resolved X-ray background intensity by stacking the X-ray spectra of detected X-ray sources, weighted by sky coverage for each source. We find that the resolved fraction of the X-ray background drops from $72 \pm 1\%$ at 0.5 – 1.0 keV to $63 \pm 4\%$ at 6.0 – 8.0 keV, consistent with previous works. The unresolved spectrum can be fitted by a powerlaw at 0.5 – 7 keV with a photon index $\Gamma = 1.22 \pm 0.04$. We also present r' band optical counterparts for 158 of the X-ray sources.

The work of JXW is supported by Chinese NSF through NSFC10473009, NSFC10533050 and the CAS “Bai Ren” project at University of Science and Technology of China.

REFERENCES

- Alexander, D. M., et al. 2003, *AJ*, 126, 539
- Bertin, E. and Arnouts, S. 1996, *A&AS* 117,393
- Brandt, W. N. & Hasinger, G. 2005, *ARA&A*, 43, 827
- De Luca, A. & Molendi, S. 2004, *A&A*, 419, 837
- Dickey, J. M. & Lockman, F. J. 1990, *ARA&A*, 28, 215
- Finkelstein, S. L., Rhoads, J. E., Malhotra, S., Pirzkal, N., Wang, J. 2007, *ApJ* in press, astro-ph/0612511
- Freeman, P.E., Kashyap, V., Rosner, R., & Lamb, D. Q. 2002, *ApJS*, 138, 185
- Giacconi, R., et al. 2002, *ApJS*, 139, 369
- Jansen, F. et al. 2001, *A&A*, 365, L1
- Kraft, R. P., Burrows, D. N., & Nousek, J. A. 1991, *ApJ*, 374, 344
- Lampton, M., Margon, B., & Bowyer, S. 1976, *ApJ*, 208, 177
- Malhotra, S., Wang, J. X., Rhoads, J. E., Heckman, T. M., & Norman, C. A. 2003, *ApJ*, 585, L25
- Manners, J. C., et al. 2003, *MNRAS*, 343, 293
- McLeod, B. A.; Gauron, T. M., Geary, J. C., Ordway, M. P., Roll, J. B. 1998, *Proc. SPIE*, 3355, 477
- Mushotzky, R. F., Cowie, L. L., Barger, A. J., & Arnaud, K. A. 2000, *Nature*, 404, 459
- Park, T., Kashyap, V. L., siemiginowska, A., van Dyk, D. A., Zezas, A., Heinke, C., & Wargelin, B. J. 2006, *ApJ*, 652, 610
- Rhoads, J. E., Malhotra, S., Dey, A., Stern, D., Spinrad, H., & Jannuzi, B. T. 2000, *ApJ*, 545, L85
- Roberts, T. P. & Warwick R. S. 2001, in *ASP Conf. Ser. 234: X-ray Astronomy 2000*, p.569
- Rosati, P., et al. 2002, *ApJ*, 566, 667
- Stern, D., et al. 2002, *AJ*, 123, 2223
- Ueda, Y., et al. 1999, *ApJ*, 518, 656
- van Dyk, D. A., Connors, A., Kashyap, V. L., & Siemiginowska, A. 2001, *ApJ*, 548, 224
- Wang, J. X. et al. 2004a, *AJ*, 127, 213
- Wang, J. X. et al. 2004b, *ApJ*, 608 L21, 213

- Wang, J. X., Malhotra, S., Rhoads, J. E., Norman, C. A. 2004c, ApJ, 612, L109
- Weisskopf, M. C., Brinkman, B., Canizares, C., Garmire, G., Murray, S., & Van Speybroeck, L. P. 2002, PASP, 114, 1
- Worsley, M. A., Fabian, A. C., Bauer, F. E., Alexander, D. M., Hasinger, G., Mateos, S., Brunner, H., Brandt, W. N., & Schneider, D. P. 2005, MNRAS, 357, 1281W
- Worsley, M. A., Fabian, A. C., Bauer, F. E., Alexander, Brandt, W. N. & Lehmer, B. D. 2006, MNRAS, 368, 1735W
- Yang, Y., Mushotzky, R. F., Barger, A. J., Cowie, L. L., Sanders, D. B., & Steffen, A. T. 2003, ApJ, 585, L85

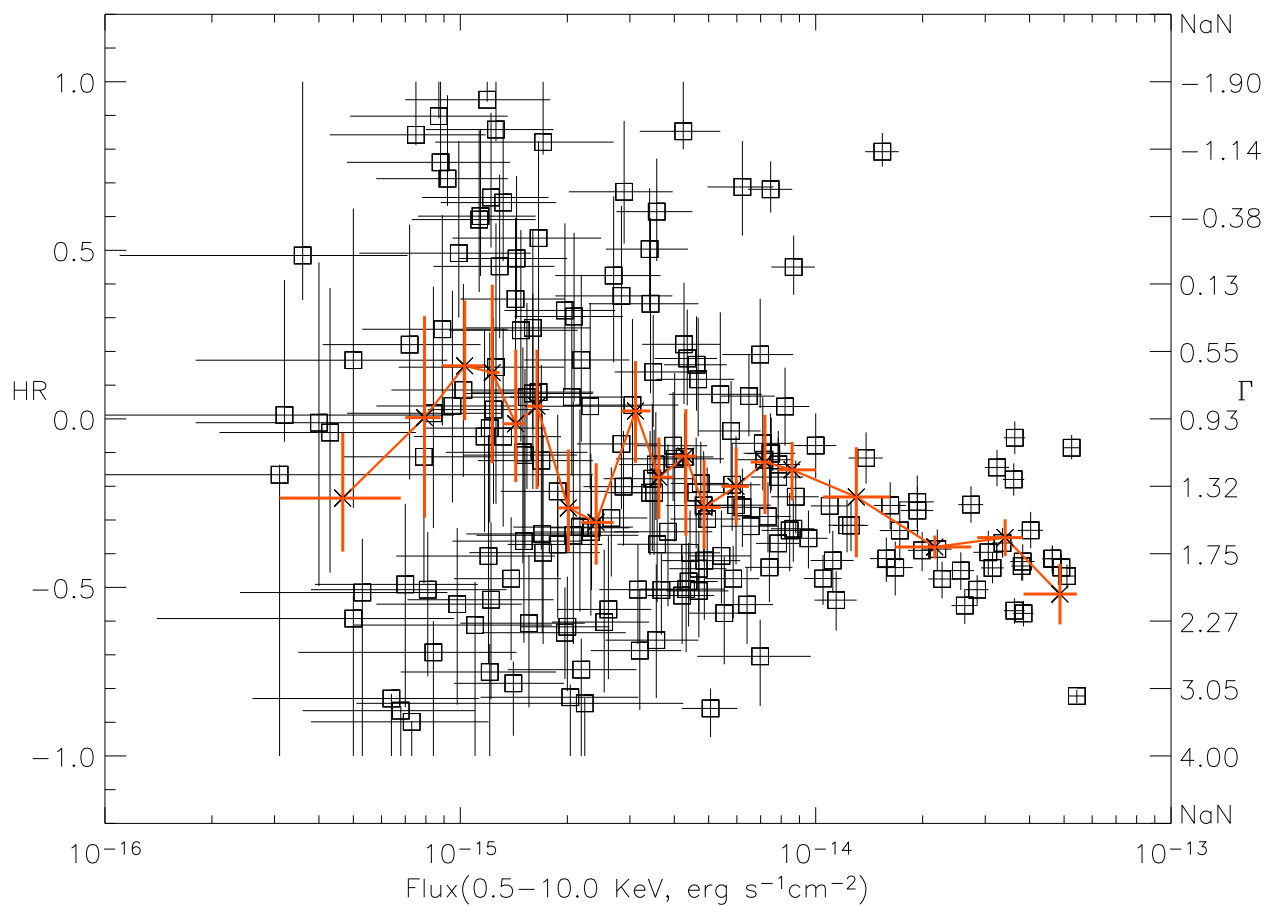


Fig. 1.— Hardness ratios $HR = (H - S)/(H + S)$ (left ordinate axis) of X-ray sources vs their full band (0.5 – 10.0 keV) X-ray fluxes. The photon indices Γ of the power-law spectra which could reproduce the observed hardness ratios are given along the right ordinate (see text for details). The line connects the average hardness ratios in different flux bins (10 sources per bin).

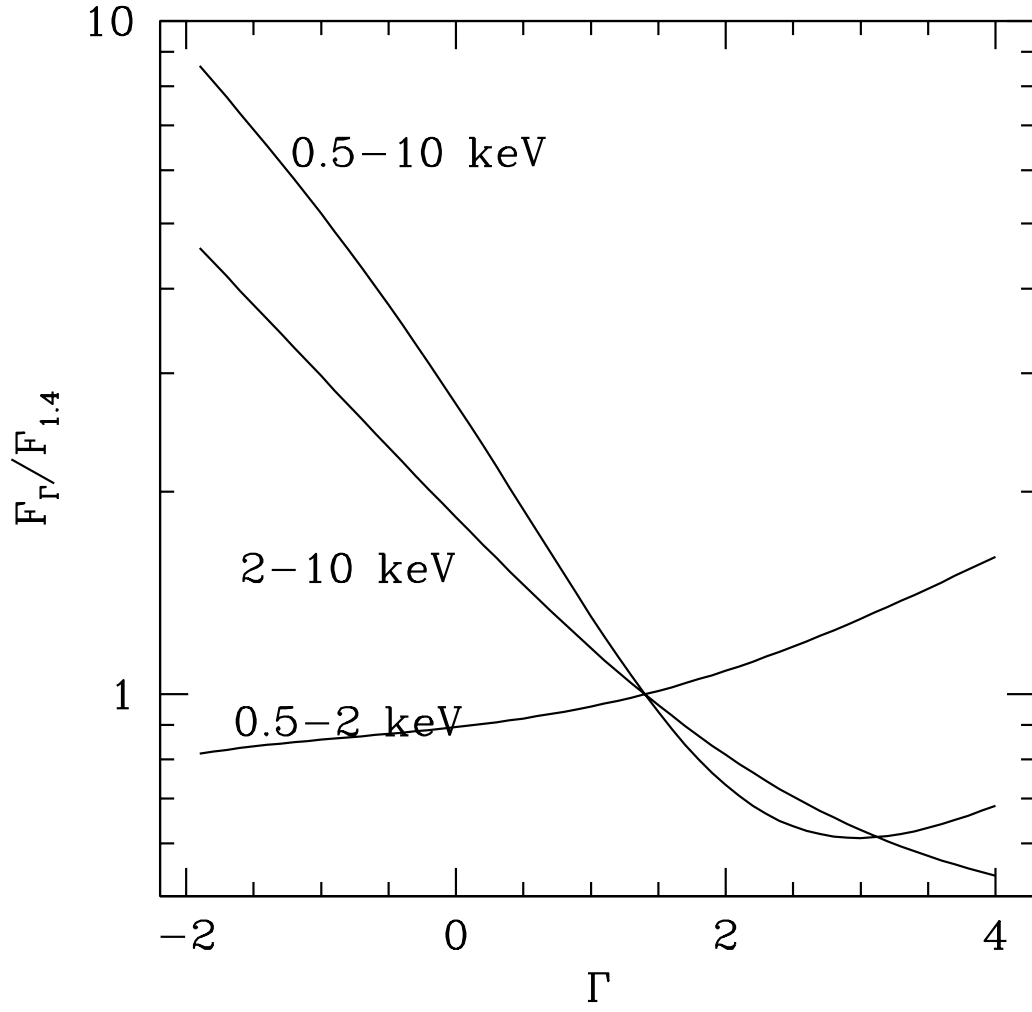


Fig. 2.— Conversion factors to calculate three band fluxes from count rates, assuming a power-law spectrum with photon index different from $\Gamma = 1.4$.

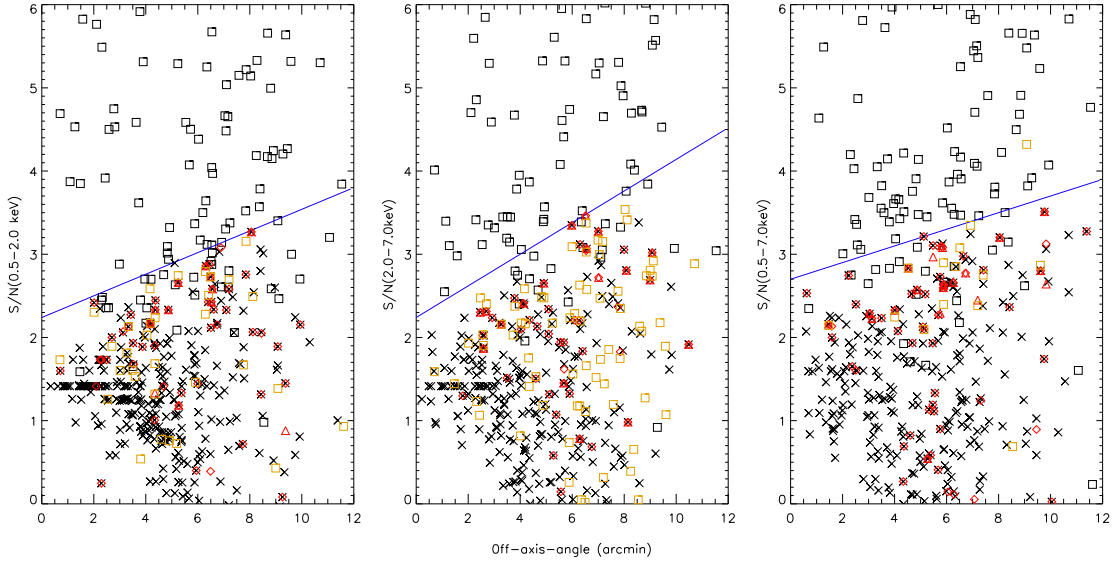


Fig. 3.— Soft (0.5 – 2.0 keV), hard (2.0 – 7.0 keV), and total (0.5 – 7.0 keV) band signal-to-noise ratio vs off-axis angle. The blue lines are the threshold we chose to build complete samples for our LogN-LogS calculation. The signal-to-noise ratios are derived from X-ray photometry (see text for details). Thus, for each source, we can give the SN ratio in each band, even it is not detected by WAVDETECT in that band. In these figures, the open black squares are sources detected in corresponding band (using WAVDETECT threshold of 10^{-7}), and other cataloged sources which are not detected in that band are plotted as yellow squares. We also plot additional sources detected by WAVDETECT but with lower thresholds (black crosses, red diamonds and red triangles with WAVDETECT thresholds of 10^{-4} , 10^{-5} and 10^{-6} respectively).

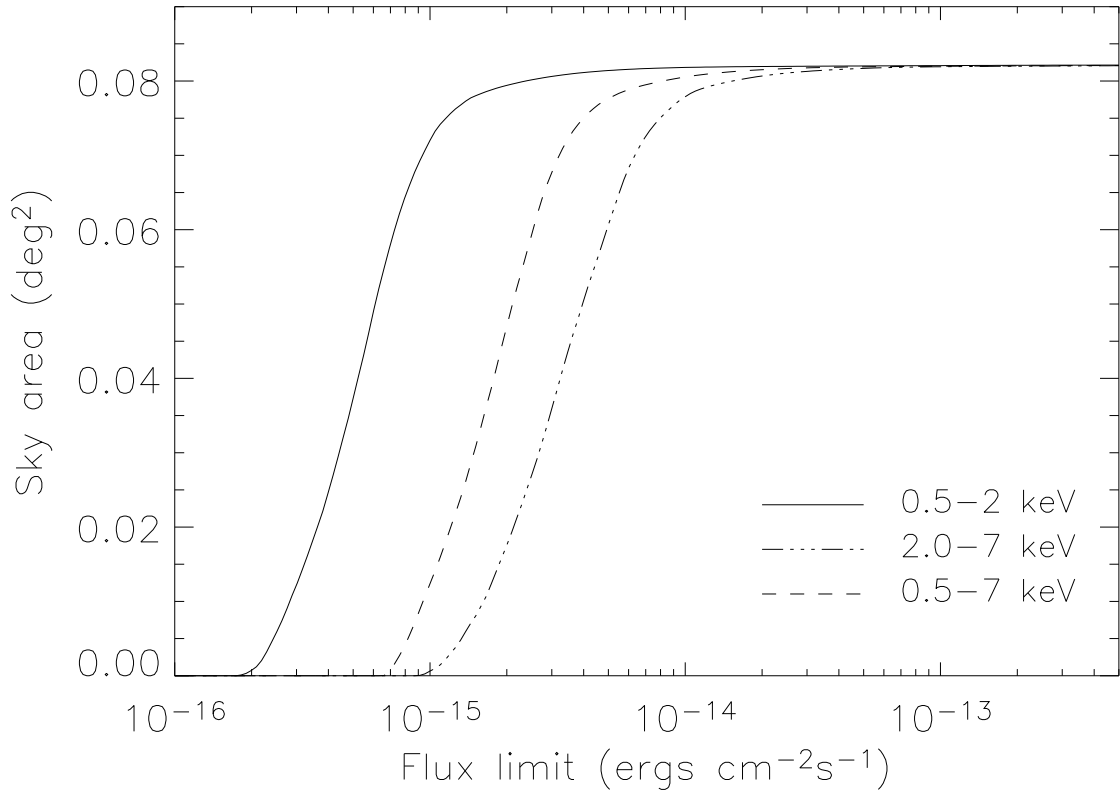


Fig. 4.— Sky coverage in soft (0.5 – 2.0 keV), hard (2.0 – 7.0 keV) and total (0.5 – 7.0 keV) bands, as a function of flux limit.

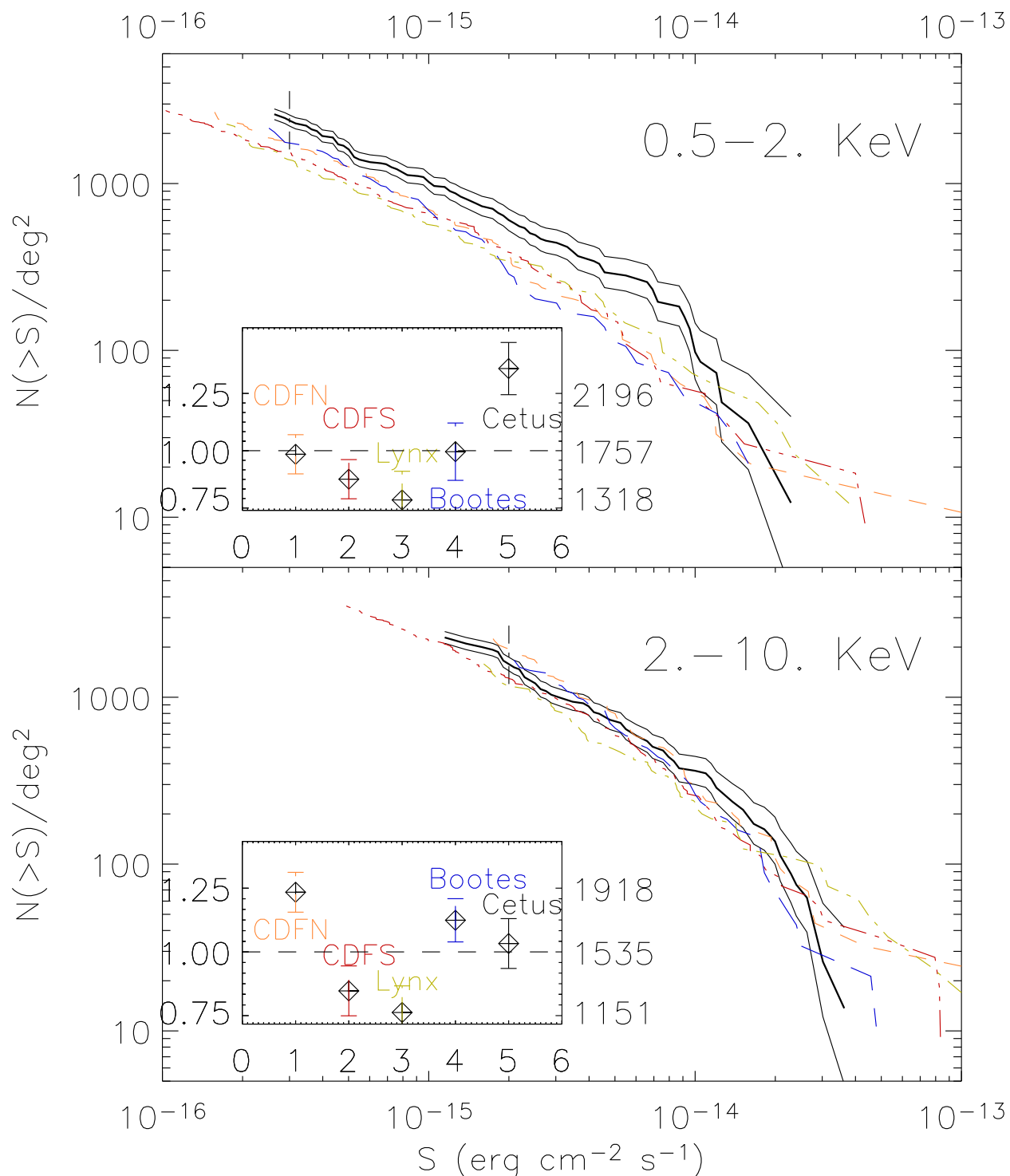


Fig. 5.— Integral source counts (LogN-LogS) in the soft (0.5 – 2.0 keV) and hard (2.0 – 10.0 keV) bands from *Chandra* observations of LALA 174 ks Cetus field, plotted as thick solid lines with two additional thin solid lines enclosing 1σ Poisson uncertainties. The LogN-LogS from the LALA 172 ks Bootes (dashed line in blue), 2 Ms CDF-N (long-dashed line in orange), 1 Ms CDF-S (dash-dotted line in red) and Lynx (dotted line in yellow) fields are also plotted. The inserts show the X-ray source densities and 1σ uncertainties from the five fields at the faint end of our 174 ks *Chandra* exposure ($3.0 \times 10^{-16} \text{ ergs cm}^{-2} \text{ s}^{-1}$ in the 0.5 – 2.0 keV band, and $2.0 \times 10^{-15} \text{ ergs cm}^{-2} \text{ s}^{-1}$ in the 2.0 – 10.0 keV band). The average source

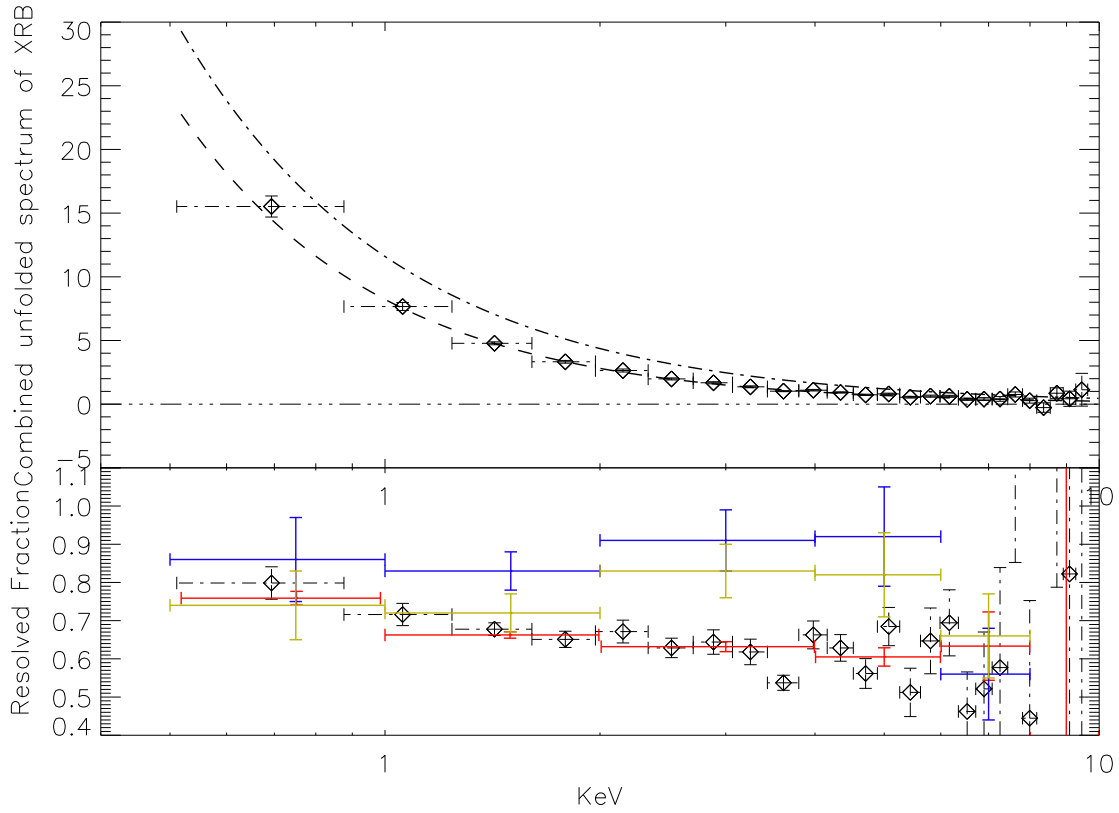


Fig. 6.— Stacked X-ray spectrum (top) and resolved fraction (bottom). The stacked spectrum is binned for display purpose, plotted with 1σ errorbars, and fitted with a powerlaw model (plotted as dashed line). The XRB model is presented as dot-dashed line. Blue and yellow data points are resolved fractions in different bands in CDF-N and CDF-S obtained by Worsley et al. (2005). Red data points are values in the Cetus field in corresponding bands.

Table 1. *Chandra* Sources in LALA Cetus Field

ID	CXOLALA2	RA(J2000)	Dec(J2000)	Err	Tot. Cts.	Soft Cts.	Hard Cts.	det	HR	S _{0.5-10} ^c	S _{0.5-2} ^c	S ₂₋₁₀ ^c	Δα(″)	Δδ(″)	r
1	J020457.9-05057.4	02:04:57.9	-05:05:7.4	0.25″	97.2 ^{+14.8} _{-13.5}	55.5 ^{+11.2} _{-9.9}	41.7 ^{+10.0} _{-8.7}	TSH	-0.14 ^{+0.10} _{-0.10}	7.85	1.88	6.55	-0.5	-0.4	21.79±0.01
2	J020456.9-050337.3	02:04:56.9	-05:03:37.3	0.15″	437.9 ^{+30.3} _{-29.2}	300.1 ^{+25.2} _{-24.1}	137.8 ^{+17.3} _{-16.0}	TSH	-0.37 ^{+0.04} _{-0.04}	33.55	9.66	20.58	-0.0	0.1	19.52±0.00
3	J020452.9-050828.9	02:04:52.9	-05:08:28.9	0.22″	140.7 ^{+17.5} _{-16.3}	88.8 ^{+14.0} _{-12.8}	51.8 ^{+10.9} _{-9.7}	TSH	-0.26 ^{+0.08} _{-0.08}	10.95	2.92	7.82	-0.1	0.2	24.25±0.07
4	J020450.2-050350.6	02:04:50.2	-05:03:50.6	0.26″	56.6 ^{+11.4} _{-10.1}	34.1 ^{+9.0} _{-7.7}	22.5 ^{+6.1} _{-5.2}	TSH	-0.20 ^{+0.12} _{-0.14}	5.82	1.47	4.52	0.2	0.1	21.99±0.01
5	J020448.2-050315.3	02:04:48.2	-05:03:15.3	0.09″	694.8 ^{+37.7} _{-37.0}	377.9 ^{+28.0} _{-27.0}	316.9 ^{+25.9} _{-24.8}	TSH	-0.09 ^{+0.04} _{-0.03}	52.52	11.98	46.74	0.2	0.1	23.25±0.04
6	J020448.1-050923.1	02:04:48.1	-05:09:23.1	0.22″	159.1 ^{+18.4} _{-17.4}	105.1 ^{+13.9} _{-13.9}	54.0 ^{+9.9} _{-9.9}	TSH	-0.32 ^{+0.07} _{-0.08}	12.57	3.51	8.24	-0.1	-0.2	20.57±0.00
7	J020447.6-050129.2	02:04:47.6	-05:01:29.2	0.29″	38.7 ^{+9.8} _{-8.5}	29.6 ^{+8.5} _{-7.2}	9.1 ^{+5.4} _{-4.1}	TSH	-0.51 ^{+0.13} _{-0.16}	3.16	1.02	1.45	0.1	0.3	22.29±0.01
8	J020447.3-050735.1	02:04:47.3	-05:07:35.1	0.43″	18.5 ^{+7.2} _{-5.8}	16.6 ^{+6.7} _{-5.4}	1.8 ^{+3.0} _{-1.8}	TS	-0.78 ^{+0.06} _{-0.16}	1.41	0.53	0.27	0.1	0.9	22.39±0.03
9	J020446.5-05044.4	02:04:46.5	-05:04:4.4	0.07″	721.5 ^{+38.4} _{-37.7}	658.0 ^{+36.9} _{-35.9}	63.6 ^{+12.0} _{-10.8}	TSH	-0.82 ^{+0.02} _{-0.02}	54.32	20.74	9.35	0.0	0.2	15.10±0.00
10	J020446.4-050155.8	02:04:46.4	-05:01:55.8	0.13″	367.6 ^{+27.7} _{-26.7}	277.3 ^{+24.1} _{-22.9}	90.3 ^{+14.1} _{-12.8}	TSH	-0.51 ^{+0.04} _{-0.05}	28.47	9.04	13.62	0.3	0.1	20.15±0.00
11	J020446.3-051022.6	02:04:46.3	-05:10:22.6	0.20″	448.1 ^{+29.6} _{-29.6}	352.3 ^{+26.1} _{-26.1}	95.8 ^{+14.7} _{-13.4}	TSH	-0.57 ^{+0.04} _{-0.04}	36.24	12.14	14.91	-0.2	-0.0	19.75±0.00
12	J020446.1-050640.7	02:04:46.1	-05:06:40.7	0.16″	99.0 ^{+14.8} _{-13.6}	15.9 ^{+6.5} _{-5.2}	83.1 ^{+13.6} _{-12.3}	TSH	0.68 ^{+0.08} _{-0.07}	7.47	0.50	12.24	0.7	0.2	21.48±0.01
13	J020445.4-050631.1	02:04:45.4	-05:06:31.1	0.26″	31.1 ^{+8.7} _{-7.4}	20.8 ^{+7.2} _{-6.8}	10.3 ^{+5.4} _{-4.3}	TSH	-0.32 ^{+0.18} _{-0.18}	2.34	0.65	1.52	0.2	-0.0	21.96±0.01
14	J020445.1-050227.9	02:04:45.1	-05:02:27.9	0.20″	124.3 ^{+16.5} _{-15.3}	84.5 ^{+13.7} _{-12.4}	39.8 ^{+9.7} _{-8.4}	TSH	-0.35 ^{+0.08} _{-0.09}	9.54	2.72	5.96	-0.1	-0.2	22.24±0.02
15	J020444.3-050625.7	02:04:44.3	-05:06:25.7	0.19″	48.8 ^{+10.5} _{-9.3}	37.0 ^{+9.3} _{-8.0}	11.8 ^{+5.6} _{-4.3}	TSH	-0.51 ^{+0.11} _{-0.16}	3.68	1.17	1.74	0.1	0.0	25.17±0.14
16	J020442.2-051041.4	02:04:42.2	-05:10:41.4	0.20″	463.0 ^{+31.2} _{-30.1}	333.2 ^{+26.4} _{-25.3}	129.8 ^{+16.9} _{-15.7}	TSH	-0.44 ^{+0.04} _{-0.04}	37.99	11.67	20.45	-0.2	0.2	19.71±0.00
17	J020441.4-05055.7	02:04:41.4	-05:05:5.7	0.24″	38.5 ^{+9.5} _{-8.2}	22.0 ^{+7.3} _{-6.0}	16.5 ^{+6.5} _{-5.2}	TSH	-0.14 ^{+0.16} _{-0.16}	3.55	0.84	2.99	0.0	0.1	25.63±0.20
18	J020441.4-050233.6	02:04:41.4	-05:02:33.6	0.39″	50.2 ^{+10.9} _{-9.5}	21.2 ^{+7.3} _{-6.0}	29.0 ^{+7.1} _{-7.1}	TSH	0.16 ^{+0.14} _{-0.14}	4.62	0.82	5.20	0.1	0.3	22.58±0.01
19	J020441.1-050942.8	02:04:41.1	-05:09:42.8	0.22″	248.2 ^{+23.0} _{-21.8}	173.1 ^{+19.2} _{-18.0}	75.2 ^{+13.1} _{-11.9}	TSH	-0.39 ^{+0.05} _{-0.06}	19.93	5.89	11.66	0.0	0.1	20.61±0.00
20	J020439.3-050414.9	02:04:39.3	-05:04:14.9	0.31″	45.3 ^{+10.5} _{-9.2}	35.0 ^{+9.1} _{-7.4}	10.3 ^{+5.6} _{-4.3}	TSH	-0.52 ^{+0.12} _{-0.12}	4.21	1.35	1.88	^a
21	J020438.9-050330.1	02:04:38.9	-05:03:30.1	0.22″	103.1 ^{+15.1} _{-13.8}	70.9 ^{+12.6} _{-11.4}	32.1 ^{+8.8} _{-7.5}	TSH	-0.37 ^{+0.09} _{-0.09}	7.84	2.25	4.79	0.4	-0.1	19.87±0.01
22	J020434.0-050643.0	02:04:34.0	-05:06:43.0	0.30″	65.0 ^{+12.1} _{-10.5}	43.5 ^{+10.0} _{-8.7}	21.5 ^{+7.3} _{-6.9}	TSH	-0.33 ^{+0.11} _{-0.11}	8.45	2.38	5.45	0.2	0.4	26.60±0.31
23	J020433.8-050450.9	02:04:33.8	-05:04:50.9	0.31″	25.8 ^{+8.5} _{-6.8}	21.1 ^{+7.3} _{-6.0}	4.7 ^{+2.9} _{-2.9}	TS	-0.62 ^{+0.15} _{-0.19}	2.00	0.68	0.71	0.1	0.2	18.12±0.00
24	J020433.5-050536.4	02:04:33.5	-05:05:36.4	0.19″	134.6 ^{+17.1} _{-15.8}	99.5 ^{+14.8} _{-13.5}	35.1 ^{+9.1} _{-7.8}	TSH	-0.47 ^{+0.07} _{-0.08}	10.49	3.24	5.35	0.1	0.0	21.93±0.01
25	J020432.6-050327.9	02:04:32.6	-05:03:27.9	0.20″	186.8 ^{+18.9} _{-18.0}	132.6 ^{+17.0} _{-15.7}	54.2 ^{+12.2} _{-9.9}	TSH	-0.41 ^{+0.06} _{-0.07}	15.80	4.70	8.94	-0.1	0.2	22.13±0.01
26	J020432.0-050724.6	02:04:32.0	-05:07:24.6	0.15″	366.3 ^{+27.7} _{-26.5}	264.5 ^{+23.5} _{-22.4}	101.8 ^{+15.0} _{-13.7}	TSH	-0.44 ^{+0.05} _{-0.05}	31.45	9.56	17.02	-0.0	-0.1	21.53±0.01
27	J020427.8-050758.1	02:04:27.8	-05:07:58.1	0.52″	89.0 ^{+14.3} _{-13.1}	58.0 ^{+11.6} _{-10.3}	31.0 ^{+8.9} _{-7.1}	TSH	-0.29 ^{+0.10} _{-0.11}	7.34	2.03	4.95	0.0	-0.2	22.14±0.02
28	J020424.0-050619.7	02:04:24.0	-05:06:19.7	0.23″	421.7 ^{+29.9} _{-28.8}	223.4 ^{+21.9} _{-20.6}	198.3 ^{+20.7} _{-19.5}	TSH	-0.06 ^{+0.05} _{-0.05}	36.32	8.14	33.05	-0.0	-0.0	18.29±0.00
29	J02058.3-05088.3	02:05:8.3	-05:08:8.3	0.29″	618.8 ^{+36.1} _{-35.2}	455.1 ^{+31.0} _{-29.8}	163.7 ^{+19.2} _{-17.9}	TSH	-0.47 ^{+0.03} _{-0.04}	50.94	16.07	25.80	0.0	-0.1	19.31±0.00
30	J02057.6-050642.2	02:05:7.6	-05:06:42.2	0.25″	565.8 ^{+35.2} _{-33.5}	401.1 ^{+34.2} _{-32.8}	164.7 ^{+19.1} _{-17.8}	TSH	-0.41 ^{+0.04} _{-0.04}	46.34	14.00	25.95	-0.2	-0.1	19.50±0.00
31	J02053.1-050639.1	02:05:3.1	-05:06:39.1	0.42″	53.4 ^{+11.4} _{-10.1}	37.9 ^{+9.5} _{-8.2}	15.6 ^{+6.9} _{-5.5}	TSH	-0.40 ^{+0.13} _{-0.14}	4.43	1.33	2.50	0.2	-0.1	23.32±0.02 ^d
32	J020459.0-050414.5	02:04:59.0	-05:04:14.5	0.42″	61.0 ^{+11.9} _{-10.7}	44.5 ^{+11.0} _{-8.8}	16.5 ^{+6.5} _{-5.5}	TSH	-0.44 ^{+0.11} _{-0.13}	4.69	1.44	2.47	-0.2	0.0	24.05±0.06
33	J020455.8-051054.2	02:04:55.8	-05:10:54.2	0.41″	195.8 ^{+20.8} _{-19.6}	123.8 ^{+16.5} _{-15.3}	72.0 ^{+13.0} _{-11.7}	TSH	-0.26 ^{+0.07} _{-0.07}	16.21	4.40	11.39	-0.1	0.0	19.75±0.00
34	J020454.2-050848.3	02:04:54.2	-05:08:48.3	0.36″	64.1 ^{+12.2} _{-10.9}	59.8 ^{+11.7} _{-10.4}	4.3 ^{+4.2} _{-2.8}	TS	-0.86 ^{+0.06} _{-0.18}	5.06	2.00	0.66	^a
35	J020453.7-05016.0	02:04:53.7	-05:01:6.0	0.61″	8.4 ^{+5.4} _{-4.1}	9.8 ^{+5.2} _{-3.9}	0.0 ^{+2.4} _{-0.0}	TS	-0.90 ^{+0.00} _{-0.10}	0.73	0.36	<0.38	-0.3	0.9	19.95±0.00
36	J020452.9-05064.6	02:04:52.9	-05:06:4.6	0.43″	8.7 ^{+5.2} _{-3.8}	6.6 ^{+4.5} _{-3.1}	2.1 ^{+3.1} _{-1.8}	TS	-0.49 ^{+0.24} _{-0.36}	0.70	0.22	0.33	0.2	0.0	22.88±0.03
37	J020450.9-050728.7	02:04:50.9	-05:07:28.7	0.40″	34.9 ^{+7.8} _{-7.8}	22.8 ^{+7.0} _{-6.1}	12.1 ^{+5.8} _{-4.5}	TSH	-0.29 ^{+0.15} _{-0.17}	2.66	0.73	1.79	0.2	0.1	24.08±0.03 ^d
38	J020446.9-050251.0	02:04:46.9	-05:02:51.0	0.46″	12.1 ^{+5.8} _{-4.5}	1.8 ^{+2.8} _{-1.4}	10.3 ^{+5.4} _{-4.1}	TH	0.71 ^{+0.25} _{-0.08}	0.92	0.06	1.53	0.2	0.2	24.58±0.08
39	J020444.6-045955.1	02:04:44.6	-04:59:55.1	0.32″	268.7 ^{+24.1} _{-22.1}	199.0 ^{+20.7} _{-19.5}	69.7 ^{+12.8} _{-11.5}	TSH	-0.48 ^{+0.05} _{-0.06}	22.68	7.13	11.37	0.1	0.0	23.27±0.04
40	J020443.2-050413.5	02:04:43.2	-05:04:13.5	0.37″	22.2 ^{+7.5} _{-6.1}	15.5 ^{+6.4} _{-5.0}	6.7 ^{+4.5} _{-3.1}	TSH	-0.37 ^{+0.17} _{-0.22}	1.88	0.55	1.12	0.2	0.3	23.04±0.04
41	J020438.3-050330.0	02:04:38.3	-05:03:30.0	0.42″	18.8 ^{+7.0} _{-6.7}	6.0 ^{+4.2} _{-2.9}	12.8 ^{+6.0} _{-4.7}	TSH	0.36 ^{+0.24} _{-0.18}	1.43	0.19	1.91	0.4	0.2	24.34±0.03 ^d
42	J020436.5-050148.4	02:04:36.5	-05:01:48.4	0.35″	67.0 ^{+12.4} _{-11.1}	49.8 ^{+10.7} _{-9.3}	17.2 ^{+5.5} _{-4.5}	TSH	-0.47 ^{+0.10} _{-0.12}	5.86	1.83	2.93	-0.0	0.1	20.55±0.00
43	J020435.1-050553.8	02:04:35.1	-05:05:53.8	0.32″	55.3 ^{+11.3} _{-10.0}	31.0 ^{+8.7} _{-7.4}	24.3 ^{+7.7} _{-6.4}	TSH	-0.11 ^{+0.13} _{-0.14}	4.28	1.00	3.67	0.7	-0.5	23.12±0.04
44	J020435.1-050631.6	02:04:35.1	-05:06:31.6	0.53″	10.3 ^{+5.4} _{-4.1}	5.8 ^{+4.2} _{-2.9}	4.5 ^{+2.6} _{-1.5}	TS	-0.10 ^{+0.31} _{-0.33}	1.50	0.35	1.29	-0.0	-0.2	25.66±0.17
45	J020434.1-050730.3	02:04:34.1	-05:07:30.3	0.50″	18.1 ^{+7.0} _{-5.7}	4.8 ^{+3.9} _{-2.6}	13.4 ^{+6.2} _{-4.8}	TH	0.48 ^{+0.24} _{-0.18}	1.44	0.16	2.06	-0.1	-0.1	21.91±0.01
46	J020433.6-050348.2	02:04:33.6	-05:03:48.2	0.46″	13.8 ^{+6.0} _{-4.7}	2.8 ^{+3.2} _{-1.9}	11.0 ^{+5.4} _{-4.1}	TH	0.60 ^{+0.26} _{-0.18}	1.14	0.10	1.77	0.5	0.4	23.82±0.08
47	J020433.5-050028.6	02:04:33.5	-05:00:28.6	0.58″	114.3 ^{+16.4} _{-15.1}	62.6 ^{+12.1} _{-10.8}	51.7 ^{+11.4} _{-10.1}	TSH	-0.08 ^{+0.10} _{-0.10}	10.00	2.32	8.76	-0.3	0.2	24.58±0.10
48	J020430.1-050453.8	02:04:30.1	-05:04:53.8	0.57″	16.7 ^{+6.9} _{-5.5}	3.3 ^{+3.6} _{-2.2}	13.4 ^{+6.2} _{-4.8}	TSH	0.64 ^{+0.24} _{-0.17}	1.32	0.11	2.07	0.2	0.1	25.37±0.18
49	J020426.3-05083.8	02:04:26.3	-05:08:3.8	0.51″	103.4 ^{+15.3} _{-14.0}	28.5 ^{+7.0} _{-6.0}	74.9 ^{+13.1} _{-11.8}	TSH	0.45 ^{+0.09} _{-0.08}	8.67	1.02	12.10	0.3	0.3	24.69±0.12
50	J020426.0-050248.5	02:04:26.0	-05:02:48.5	0.21″	468.2 ^{+31.3} _{-30.4}	370.1 ^{+27.9} _{-26.9}	98.0 ^{+14.9} _{-13.6}	TSH							

Table 1—Continued

ID	CXOLALA2	RA(J2000)	Dec(J2000)	Err	Tot. Cts.	Soft Cts.	Hard Cts.	det	HR	S _{0.5–10} ^c	S _{0.5–2} ^e	S _{2–10} ^e	$\Delta\alpha(^{\prime\prime})$	$\Delta\delta(^{\prime\prime})$	r
52	J020420.1-05063.6	02:04:20.1	-05:06:3.6	0.38''	425.3 ^{+30.0}	251.7 ^{+23.1}	173.6 ^{+19.5}	TSH	-0.18 ^{+0.05}	36.08	9.10	28.33	-0.1	0.4	19.60±0.00
53	J020518.4-050457.9	02:05:18.4	-05:04:57.9	0.79''	304.7 ^{+26.2}	238.7 ^{+22.7}	66.0 ^{+13.5}	TSH	-0.55 ^{+0.05}	26.28	8.95	10.78	0.1	-0.0	19.20±0.00
54	J020514.6-050954.3	02:05:14.6	-05:09:54.3	0.68''	202.7 ^{+21.8}	130.3 ^{+17.2}	72.4 ^{+13.9}	TSH	-0.27 ^{+0.07}	19.33	5.45	12.97	0.1	-0.7	22.45±0.02
55	J02057.8-050157.0	02:05:7.8	-05:01:57.0	0.52''	325.3 ^{+26.7}	205.6 ^{+20.1}	119.7 ^{+15.4}	TSH	-0.25 ^{+0.05}	27.36	7.39	19.37	0.3	-0.1	21.00±0.00 ^d
56	J02056.9-050314.2	02:05:6.9	-05:03:14.2	0.58''	152.1 ^{+18.5}	100.9 ^{+15.0}	51.2 ^{+11.3}	TSH	-0.32 ^{+0.08}	12.25	3.46	7.96	-0.1	0.2	22.07±0.03 ^d
57	J02054.0-050830.0	02:05:4.0	-05:08:30.0	0.78''	77.0 ^{+13.7}	49.4 ^{+10.7}	27.6 ^{+8.9}	TSH	-0.26 ^{+0.11}	6.22	1.70	4.29	>25.86
58	J02053.6-050442.5	02:05:3.6	-05:04:42.5	0.59''	56.1 ^{+11.6}	42.1 ^{+9.9}	14.0 ^{+6.5}	TSH	-0.48 ^{+0.11}	4.39	1.39	2.12	-0.1	-0.1	20.63±0.00
59	J020454.7-051014.6	02:04:54.7	-05:10:14.6	0.63''	91.3 ^{+14.6}	66.4 ^{+12.4}	24.8 ^{+8.3}	TSH	-0.44 ^{+0.09}	7.41	2.30	3.87	-0.2	-0.2	20.75±0.01
60	J020452.2-05097.9	02:04:52.2	-05:09:7.9	0.61''	6.4 ^{+5.3}	3.2 ^{+4.0}	3.2 ^{+3.8}	T	0.17 ^{+0.45}	0.50	0.11	0.48	0.3	0.4	18.07±0.00
61	J020451.6-050654.2	02:04:51.6	-05:06:54.2	0.63''	12.3 ^{+5.8}	5.8 ^{+4.2}	6.5 ^{+4.5}	TS	0.08 ^{+0.30}	1.60	0.32	1.66	-0.3	0.4	25.43±0.14
62	J020450.9-050126.9	02:04:50.9	-05:01:26.9	0.58''	14.9 ^{+4.5}	8.1 ^{+2.9}	6.8 ^{+3.1}	TS	-0.05 ^{+0.28}	1.17	0.27	1.04	-0.1	0.3	22.65±0.02
63	J020450.7-045618.9	02:04:50.7	-04:56:18.9	0.67''	516.4 ^{+33.9}	368.3 ^{+28.1}	148.1 ^{+19.2}	TSH	-0.42 ^{+0.04}	46.34	14.47	25.06	0.3	0.8	21.24±0.01
64	J020448.6-050213.2	02:04:48.6	-05:02:13.2	0.57''	9.3 ^{+5.4}	4.1 ^{+3.6}	5.3 ^{+4.2}	T	0.22 ^{+0.36}	0.72	0.13	0.80	0.9	0.6	23.60±0.05
65	J020448.0-050138.4	02:04:48.0	-05:01:38.4	0.46''	58.4 ^{+11.6}	35.0 ^{+9.0}	23.4 ^{+7.7}	TSH	-0.19 ^{+0.12}	4.75	1.20	3.70	-0.6	0.7	22.07±0.02
66	J020445.2-045716.4	02:04:45.2	-04:57:16.4	0.79''	277.3 ^{+24.9}	202.7 ^{+21.0}	74.6 ^{+13.9}	TSH	-0.45 ^{+0.05}	25.61	8.11	13.11	0.1	0.3	21.05±0.01
67	J020443.2-051116.7	02:04:43.2	-05:11:16.7	0.81''	56.3 ^{+11.9}	43.2 ^{+10.2}	13.1 ^{+6.4}	TS	-0.51 ^{+0.12}	4.69	1.54	2.09	-0.0	0.1	21.54±0.01
68	J020440.4-051138.4	02:04:40.4	-05:11:38.4	1.11''	21.7 ^{+8.4}	7.9 ^{+5.2}	13.8 ^{+7.0}	TH	0.32 ^{+0.26}	1.97	0.31	2.38	0.4	0.1	19.66±0.00
69	J020438.7-045825.1	02:04:38.7	-04:58:25.1	1.17''	75.3 ^{+13.8}	59.4 ^{+11.8}	15.9 ^{+5.7}	TS	-0.55 ^{+0.11}	6.41	2.18	2.59	0.2	0.1	21.70±0.01
70	J020437.0-050314.1	02:04:37.0	-05:03:14.1	0.62''	10.1 ^{+5.4}	3.8 ^{+3.6}	6.4 ^{+4.5}	T	0.27 ^{+0.34}	0.89	0.14	1.09	0.5	0.8	22.37±0.02
71	J020437.0-051136.9	02:04:37.0	-05:11:36.9	0.62''	180.9 ^{+19.0}	19.5 ^{+7.6}	161.4 ^{+18.9}	TSH	0.79 ^{+0.06}	15.40	0.71	26.17	0.8	0.2	20.63±0.01
72	J020436.8-050017.8	02:04:36.8	-05:00:17.8	0.48''	105.9 ^{+15.6}	70.9 ^{+12.7}	35.0 ^{+9.5}	TSH	-0.33 ^{+0.09}	8.65	2.46	5.53	-0.2	0.3	19.21±0.00
73	J020436.7-051034.4	02:04:36.7	-05:10:34.4	0.61''	90.3 ^{+14.5}	50.4 ^{+10.8}	39.9 ^{+10.1}	TSH	-0.10 ^{+0.11}	7.50	1.79	6.36	-1.0	0.5	21.26±0.01
74	J020434.4-050332.8	02:04:34.4	-05:03:32.8	0.60''	8.8 ^{+4.1}	9.1 ^{+5.2}	0.0 ^{+2.6}	TS	-0.87 ^{+0.01}	0.68	0.30	<0.39	-0.0	0.1	24.01±0.02 ^d
75	J020433.9-051544.3	02:04:33.9	-05:15:44.3	0.92''	359.1 ^{+28.9}	257.3 ^{+23.6}	101.7 ^{+17.3}	TSH	-0.42 ^{+0.05}	38.24	12.38	19.77	^b
76	J020429.9-050557.7	02:04:29.9	-05:05:57.7	0.72''	15.3 ^{+6.9}	3.1 ^{+3.6}	12.2 ^{+6.2}	TH	0.66 ^{+0.25}	1.22	0.10	1.90	1.0	0.4	25.60±0.20
77	J020429.5-050534.0	02:04:29.5	-05:05:34.0	0.37''	35.3 ^{+9.4}	21.5 ^{+7.3}	13.8 ^{+6.4}	TSH	-0.20 ^{+0.17}	2.88	0.74	2.19	0.1	0.1	19.53±0.00
78	J020428.9-050727.5	02:04:28.9	-05:07:27.5	0.72''	19.3 ^{+7.2}	3.4 ^{+3.6}	16.0 ^{+6.5}	TH	0.67 ^{+0.21}	2.89	0.21	4.62	0.2	-0.3	19.61±0.00
79	J020417.3-050126.2	02:04:17.3	-05:01:26.2	0.72''	347.2 ^{+27.7}	200.1 ^{+19.7}	147.1 ^{+18.5}	TSH	-0.14 ^{+0.05}	32.38	8.06	26.12	-0.1	0.6	22.64±0.02
80	J020415.0-050514.5	02:04:15.0	-05:05:14.5	0.65''	231.5 ^{+22.7}	161.5 ^{+18.9}	70.0 ^{+13.0}	TSH	-0.39 ^{+0.06}	21.99	6.61	12.66	-0.4	0.0	19.76±0.00
81	J02045.6-050134.5	02:04:5.6	-05:01:34.5	0.86''	474.5 ^{+21.4}	344.4 ^{+17.6}	130.1 ^{+11.7}	TSH	-0.44 ^{+0.07}	49.15	15.85	24.99	-0.2	-0.0	22.32±0.02
82	J020520.6-05039.6	02:05:20.6	-05:03:9.6	1.21''	189.0 ^{+21.5}	119.6 ^{+16.5}	69.4 ^{+14.1}	TSH	-0.25 ^{+0.08}	19.31	5.35	13.36	-0.9	0.4	21.57±0.01
83	J02058.3-050921.1	02:05:8.3	-05:09:21.1	1.26''	61.3 ^{+12.9}	44.1 ^{+10.6}	17.2 ^{+6.6}	TSH	-0.41 ^{+0.13}	5.43	1.69	2.90	0.1	-0.2	21.69±0.01
84	J02056.8-05065.3	02:05:6.8	-05:06:5.3	0.78''	54.4 ^{+11.7}	23.0 ^{+7.9}	31.5 ^{+9.0}	TSH	0.18 ^{+0.14}	4.35	0.78	4.85	0.2	0.2	20.59±0.00
85	J02050.9-050951.5	02:05:0.9	-05:09:51.5	1.26''	17.8 ^{+10.4}	14.4 ^{+6.5}	3.3 ^{+4.7}	TS	-0.61 ^{+0.20}	1.56	0.54	0.56	-0.8	-0.6	23.10±0.03
86	J02050.6-045551.7	02:05:0.6	-04:55:51.7	1.12''	328.6 ^{+27.3}	220.3 ^{+22.1}	108.2 ^{+16.7}	TSH	-0.33 ^{+0.05}	40.27	11.97	24.73	0.4	-0.1	19.20±0.00
87	J02050.6-050927.8	02:05:0.6	-05:09:27.8	1.04''	19.1 ^{+8.2}	9.4 ^{+5.6}	9.7 ^{+6.3}	TSH	0.08 ^{+0.30}	1.66	0.35	1.61	-0.5	-0.9	24.84±0.12
88	J020452.4-05084.5	02:04:52.4	-05:08:4.5	0.66''	14.6 ^{+6.8}	3.6 ^{+4.3}	11.1 ^{+5.0}	TH	0.59 ^{+0.22}	1.13	0.12	1.66	-0.3	-0.0	22.28±0.01 ^d
89	J020451.4-050157.8	02:04:51.4	-05:01:57.8	0.80''	13.1 ^{+6.2}	6.0 ^{+4.2}	7.1 ^{+5.0}	TS	0.09 ^{+0.31}	1.02	0.20	1.08	0.2	0.2	19.15±0.00
90	J020448.2-045723.8	02:04:48.2	-04:57:23.8	1.11''	116.8 ^{+16.9}	84.3 ^{+13.9}	32.5 ^{+10.0}	TSH	-0.42 ^{+0.09}	11.17	3.49	5.93	0.1	0.5	22.32±0.03
91	J020445.0-04572.2	02:04:45.0	-04:57:2.2	1.15''	125.3 ^{+17.8}	98.0 ^{+15.1}	27.4 ^{+9.8}	TSH	-0.54 ^{+0.09}	11.42	3.88	4.73	-0.4	0.3	22.38±0.02
92	J020444.5-050915.5	02:04:44.5	-05:09:15.5	0.49''	15.3 ^{+6.7}	8.1 ^{+5.0}	7.2 ^{+5.0}	TSH	-0.03 ^{+0.28}	1.21	0.27	1.10	-0.3	-0.4	21.16±0.01
93	J020442.2-050926.6	02:04:42.2	-05:09:26.6	0.77''	10.5 ^{+5.8}	5.3 ^{+4.2}	5.2 ^{+4.5}	TH	0.02 ^{+0.38}	0.84	0.18	0.80	-0.6	-0.7	19.56±0.00
94	J020440.9-050045.3	02:04:40.9	-05:00:45.3	0.96''	4.5 ^{+4.4}	1.1 ^{+2.7}	3.4 ^{+3.9}	T	0.48 ^{+0.52}	0.36	0.04	0.53	>25.86
95	J020440.6-051024.0	02:04:40.6	-05:10:24.0	0.87''	10.8 ^{+3.1}	1.5 ^{+1.1}	9.4 ^{+2.4}	TH	0.76 ^{+0.24}	0.88	0.05	1.47	0.5	0.5	23.53±0.05
96	J020438.3-05093.5	02:04:38.3	-05:09:3.5	0.62''	11.9 ^{+6.0}	5.8 ^{+4.2}	6.1 ^{+4.7}	TS	0.04 ^{+0.34}	0.95	0.20	0.95	-0.1	-0.3	23.59±0.05
97	J020433.5-045838.7	02:04:33.5	-04:58:38.7	1.41''	39.7 ^{+10.8}	25.1 ^{+8.3}	14.6 ^{+7.5}	TSH	-0.22 ^{+0.18}	3.42	0.93	2.41	>25.86
98	J020431.3-050132.2	02:04:31.3	-05:01:32.2	0.80''	19.9 ^{+7.5}	12.4 ^{+6.0}	7.4 ^{+5.0}	TS	-0.22 ^{+0.23}	1.88	0.50	1.37	0.3	-0.0	19.66±0.00
99	J020427.9-05052.8	02:04:27.9	-05:05:2.8	0.93''	16.0 ^{+6.9}	4.5 ^{+3.9}	11.4 ^{+6.0}	TH	0.45 ^{+0.27}	1.29	0.15	1.79	0.7	0.4	22.11±0.02
100	J020427.1-050620.3	02:04:27.1	-05:06:20.3	0.75''	15.7 ^{+5.0}	6.3 ^{+4.7}	9.4 ^{+5.6}	TH	0.27 ^{+0.29}	1.60	0.27	1.86	>25.86
101	J020426.5-050340.1	02:04:26.5	-05:03:40.1	0.96''	18.4 ^{+7.6}	9.1 ^{+5.4}	9.3 ^{+5.8}	TSH	0.06 ^{+0.28}	1.54	0.32	1.50	>25.86

Table 1—Continued

ID	CXOLALA2	RA(J2000)	Dec(J2000)	Err	Tot. Cts.	Soft Cts.	Hard Cts.	det	HR	S _{0.5–10} ^e	S _{0.5–2} ^e	S _{2–10} ^e	Δα('')	Δδ('')	r
103	J020419.3-050145.8	02:04:19.3	-05:01:45.8	1.17''	41.2 ^{+10.7} _{-9.3}	28.9 ^{+8.8} _{-7.5}	12.2 ^{+6.5} _{-5.2}	TSH	-0.37 ^{+0.16} _{-0.17}	3.58	1.08	2.04	-0.1	1.1	21.07±0.00
104	J020416.5-050648.5	02:04:16.5	-05:06:48.5	0.85''	85.2 ^{+14.8} _{-13.6}	48.2 ^{+11.0} _{-9.7}	37.0 ^{+10.3} _{-9.1}	TSH	-0.10 ^{+0.12} _{-0.12}	7.46	1.81	6.19	-0.4	-0.1	22.89±0.03
105	J020415.9-05075.9	02:04:15.9	-05:07:5.9	1.15''	89.1 ^{+15.2} _{-13.9}	44.2 ^{+10.7} _{-9.4}	44.9 ^{+11.1} _{-9.8}	TSH	0.04 ^{+0.12} _{-0.12}	8.20	1.75	7.87	-0.0	-0.3	22.20±0.02
106	J02047.2-050450.1	02:04:7.2	-05:04:50.1	1.40''	171.4 ^{+20.7} _{-19.5}	125.4 ^{+17.0} _{-15.7}	45.9 ^{+12.3} _{-11.0}	TSH	-0.44 ^{+0.08} _{-0.08}	16.74	5.38	8.40	0.2	-0.2	21.76±0.01
107	J02044.7-050120.4	02:04:4.7	-05:01:20.4	0.78''	252.3 ^{+24.5} _{-23.3}	177.6 ^{+20.0} _{-18.9}	74.8 ^{+14.5} _{-13.3}	TSH	-0.40 ^{+0.06} _{-0.07}	30.71	9.61	16.76	0.3	0.9	18.61±0.00
108	J020521.8-050515.3	02:05:21.8	-05:05:15.3	2.16''	54.9 ^{+14.4} _{-13.2}	40.6 ^{+10.9} _{-9.5}	14.3 ^{+9.8} _{-8.6}	TS	-0.42 ^{+0.22} _{-0.18}	4.86	1.58	2.37	0.4	1.0	24.20±0.09
109	J020520.2-05040.9	02:05:20.2	-05:04:0.9	2.13''	48.4 ^{+13.1} _{-11.8}	6.0 ^{+6.3} _{-5.1}	42.3 ^{+11.5} _{-10.2}	TH	0.85 ^{+0.15} _{-0.05}	4.24	0.23	7.00	1.3	-0.5	22.75±0.03
110	J020518.7-05072.1	02:05:18.7	-05:07:2.1	1.60''	62.3 ^{+13.9} _{-12.6}	11.8 ^{+7.2} _{-5.8}	50.4 ^{+12.2} _{-10.9}	TSH	0.69 ^{+0.14} _{-0.14}	6.22	0.52	9.49	-0.3	-0.6	21.20±0.01
111	J020514.3-050419.6	02:05:14.3	-05:04:19.6	1.67''	36.4 ^{+11.1} _{-9.8}	31.3 ^{+9.3} _{-8.0}	5.1 ^{+5.8} _{-4.8}	TS	-0.69 ^{+0.18} _{-0.18}	3.20	1.19	0.85	0.2	-0.4	21.78±0.01
112	J020513.7-050942.9	02:05:13.7	-05:09:42.9	1.18''	59.7 ^{+13.6} _{-12.4}	48.2 ^{+11.2} _{-9.9}	11.5 ^{+8.2} _{-6.9}	TS	-0.58 ^{+0.17} _{-0.15}	5.53	1.95	2.01	0.0	-0.9	22.76±0.03
113	J020512.0-05019.8	02:05:12.0	-05:01:9.8	1.14''	77.0 ^{+14.4} _{-13.7}	52.7 ^{+11.7} _{-10.4}	24.4 ^{+9.8} _{-8.5}	TSH	-0.32 ^{+0.13} _{-0.13}	6.57	1.94	3.96	-0.2	0.4	24.03±0.03 ^d
114	J020510.4-05036.1	02:05:10.4	-05:03:6.1	1.30''	43.3 ^{+11.2} _{-9.9}	9.4 ^{+5.8} _{-4.5}	33.9 ^{+9.9} _{-8.6}	TSH	0.61 ^{+0.16} _{-0.15}	3.57	0.33	5.36	>25.86
115	J02054.8-050442.5	02:05:4.8	-05:04:42.5	1.19''	6.2 ^{+5.8} _{-4.6}	6.6 ^{+5.2} _{-4.0}	0.0 ^{+0.8} _{-0.0}	TS	-0.59 ^{+0.07} _{-0.11}	0.50	0.22	<0.57	0.2	-0.2	23.13±0.04
116	J02053.1-050127.4	02:05:3.1	-05:01:27.4	1.11''	20.8 ^{+8.3} _{-7.0}	12.3 ^{+6.2} _{-4.8}	8.6 ^{+6.0} _{-4.7}	TS	-0.12 ^{+0.28} _{-0.26}	1.69	0.42	1.34	>25.86
117	J02052.8-050346.0	02:05:2.8	-05:03:46.0	0.95''	14.8 ^{+6.7} _{-5.4}	1.1 ^{+2.7} _{-1.4}	13.7 ^{+6.4} _{-5.4}	TH	0.86 ^{+0.14} _{-0.03}	1.26	0.04	2.27	0.4	-0.7	26.26±0.26
118	J02051.3-045938.9	02:05:1.3	-04:59:38.9	0.97''	31.2 ^{+10.0} _{-8.7}	25.0 ^{+8.5} _{-7.2}	6.3 ^{+5.7} _{-4.4}	TS	-0.57 ^{+0.22} _{-0.21}	2.61	0.90	1.00	-0.2	1.3	22.74±0.02
119	J02050.5-05062.6	02:05:0.5	-05:06:2.6	0.67''	14.6 ^{+6.4} _{-5.0}	7.3 ^{+4.7} _{-3.4}	7.3 ^{+4.7} _{-3.4}	T	0.03 ^{+0.27} _{-0.28}	1.24	0.26	1.20	0.0	0.7	23.91±0.06
120	J020458.9-050443.3	02:04:58.9	-05:04:43.3	0.53''	18.1 ^{+5.5} _{-5.5}	13.5 ^{+4.7} _{-4.2}	4.5 ^{+2.6} _{-2.6}	TS	-0.47 ^{+0.18} _{-0.24}	1.39	0.44	0.68	^a
121	J020443.1-050556.7	02:04:43.1	-05:05:56.7	0.98''	5.7 ^{+4.2} _{-2.9}	3.0 ^{+3.2} _{-1.9}	2.7 ^{+3.2} _{-1.9}	T	-0.04 ^{+0.43} _{-0.42}	0.43	0.09	0.41	>25.86
122	J020441.8-045638.2	02:04:41.8	-04:56:38.2	1.38''	79.7 ^{+13.8} _{-13.8}	46.2 ^{+11.0} _{-9.4}	33.5 ^{+10.6} _{-9.4}	TSH	-0.12 ^{+0.15} _{-0.15}	7.17	1.81	5.69	>25.86
123	J020439.1-050341.8	02:04:39.1	-05:03:41.8	0.76''	10.4 ^{+5.6} _{-4.3}	6.1 ^{+4.5} _{-3.1}	4.3 ^{+3.9} _{-2.6}	T	-0.11 ^{+0.32} _{-0.38}	0.79	0.19	0.64	^a
124	J020436.3-050833.9	02:04:36.3	-05:08:33.9	0.89''	9.4 ^{+5.4} _{-4.8}	0.5 ^{+2.4} _{-1.5}	8.8 ^{+5.2} _{-3.9}	TH	0.84 ^{+0.16} _{-0.03}	0.75	0.02	1.37	0.1	0.3	23.31±0.05
125	J020433.7-045929.9	02:04:33.7	-04:59:29.9	1.06''	44.9 ^{+10.5} _{-9.5}	29.7 ^{+8.7} _{-7.4}	15.2 ^{+5.7} _{-5.7}	TSH	-0.30 ^{+0.15} _{-0.16}	4.95	1.41	3.21	^a
126	J020432.4-045748.0	02:04:32.4	-04:57:48.0	1.43''	52.0 ^{+12.5} _{-11.2}	32.9 ^{+9.7} _{-8.4}	19.1 ^{+8.3} _{-7.0}	TS	-0.22 ^{+0.16} _{-0.17}	3.61	1.27	3.21	-0.2	0.2	22.12±0.02
127	J020431.6-051421.3	02:04:31.6	-05:14:21.3	1.38''	45.9 ^{+13.0} _{-11.8}	34.9 ^{+9.9} _{-8.6}	11.0 ^{+7.4} _{-7.4}	TS	-0.51 ^{+0.25} _{-0.19}	4.32	1.46	1.92	^b
128	J020431.1-051058.3	02:04:31.1	-05:10:58.3	1.27''	24.3 ^{+8.9} _{-7.6}	10.8 ^{+6.0} _{-4.7}	13.5 ^{+7.0} _{-5.7}	TS	0.17 ^{+0.25} _{-0.24}	2.19	0.42	2.32	0.4	-0.4	18.06±0.00
129	J020430.4-050846.4	02:04:30.4	-05:08:46.4	1.40''	11.9 ^{+6.2} _{-4.8}	9.3 ^{+5.2} _{-3.9}	2.6 ^{+3.6} _{-2.4}	TS	-0.55 ^{+0.23} _{-0.30}	0.98	0.32	0.42	-0.3	0.3	23.11±0.04
130	J020428.4-050227.8	02:04:28.4	-05:02:27.8	1.00''	18.7 ^{+7.5} _{-6.1}	10.9 ^{+5.8} _{-4.5}	7.9 ^{+5.2} _{-3.9}	TS	-0.11 ^{+0.26} _{-0.28}	1.52	0.37	1.24	>25.86
131	J020427.6-051227.0	02:04:27.6	-05:12:27.0	1.74''	24.3 ^{+10.5} _{-9.2}	22.5 ^{+8.3} _{-7.0}	1.7 ^{+6.6} _{-1.7}	TS	-0.74 ^{+0.09} _{-0.26}	1.29	0.89	0.29	-1.2	-0.4	22.78±0.03
132	J020427.4-045842.3	02:04:27.4	-04:58:42.3	0.93''	100.4 ^{+12.1} _{-14.8}	63.3 ^{+12.5} _{-11.2}	37.1 ^{+10.5} _{-9.2}	TSH	-0.23 ^{+0.11} _{-0.11}	8.79	2.39	6.20	^a
133	J020425.9-050153.5	02:04:25.9	-05:01:53.5	1.10''	42.0 ^{+10.5} _{-9.3}	18.7 ^{+7.2} _{-5.8}	23.3 ^{+8.2} _{-6.8}	TSH	0.14 ^{+0.17} _{-0.16}	3.49	0.66	3.74	1.1	0.3	23.02±0.06
134	J020425.1-050044.8	02:04:25.1	-05:00:44.8	0.89''	72.7 ^{+13.3} _{-12.0}	34.5 ^{+9.3} _{-8.0}	38.2 ^{+9.9} _{-8.6}	TSH	0.07 ^{+0.12} _{-0.12}	6.49	1.31	6.55	0.0	-0.4	16.27±0.00
135	J020419.9-050510.0	02:04:19.9	-05:05:10.0	1.22''	16.0 ^{+8.8} _{-7.5}	21.0 ^{+7.5} _{-6.1}	4.9 ^{+5.0} _{-3.8}	TS	-0.60 ^{+0.21} _{-0.21}	2.54	0.88	0.93	0.0	-0.4	20.22±0.00
136	J020419.3-050630.4	02:04:19.3	-05:06:30.4	1.22''	23.0 ^{+7.3} _{-6.0}	9.7 ^{+5.6} _{-4.3}	3.7 ^{+4.6} _{-3.5}	T	-0.41 ^{+0.36} _{-0.32}	1.20	0.37	0.64	^a
137	J020418.8-050447.7	02:04:18.8	-05:04:47.7	1.10''	23.6 ^{+8.5} _{-7.2}	16.3 ^{+7.5} _{-5.7}	7.3 ^{+5.4} _{-4.1}	TS	-0.34 ^{+0.23} _{-0.25}	2.33	0.69	1.38	-0.3	-0.3	23.55±0.02 ^d
138	J020413.5-050717.0	02:04:13.5	-05:07:17.0	1.20''	86.9 ^{+15.3} _{-14.1}	52.5 ^{+11.7} _{-10.4}	34.4 ^{+10.3} _{-9.0}	TSH	-0.17 ^{+0.12} _{-0.12}	7.84	2.05	5.89	-0.4	-0.2	22.24±0.02
139	J020528.5-050553.4	02:05:28.5	-05:05:53.4	1.85''	9.6 ^{+8.6} _{-7.4}	15.0 ^{+6.0} _{-5.0}	0.0 ^{+0.5} _{-0.0}	TS	-0.84 ^{+0.02} _{-0.16}	2.24	1.57	<0.90	0.9	-1.1	23.58±0.05 ^c
140	J020518.7-050216.6	02:05:18.7	-05:02:16.6	1.00''	145.7 ^{+19.1} _{-17.9}	98.8 ^{+15.2} _{-13.9}	46.9 ^{+12.1} _{-10.7}	TSH	-0.33 ^{+0.09} _{-0.09}	17.25	5.10	10.50	>25.86
141	J020515.5-050545.9	02:05:15.5	-05:05:45.9	1.30''	49.4 ^{+12.0} _{-10.7}	32.2 ^{+9.4} _{-7.7}	17.3 ^{+8.0} _{-6.7}	TSH	-0.26 ^{+0.16} _{-0.16}	4.84	1.36	3.22	1.1	-0.5	25.00±0.07 ^d
142	J02059.1-05039.8	02:05:9.1	-05:03:9.8	1.44''	21.4 ^{+8.4} _{-7.1}	10.5 ^{+5.6} _{-4.3}	10.9 ^{+6.7} _{-5.4}	TS	0.06 ^{+0.28} _{-0.23}	2.06	0.43	2.03	-1.2	0.9	25.26±0.15
143	J02057.8-050119.4	02:05:7.8	-05:01:19.4	1.90''	22.0 ^{+8.3} _{-7.0}	12.8 ^{+6.2} _{-4.7}	9.2 ^{+6.0} _{-4.7}	TS	-0.12 ^{+0.25} _{-0.25}	4.01	1.00	3.23	-1.1	-1.0	26.68±0.23
144	J02055.7-050743.1	02:05:5.7	-05:07:43.1	1.50''	11.6 ^{+6.8} _{-5.5}	3.9 ^{+4.3} _{-3.1}	7.7 ^{+5.6} _{-4.3}	T	0.49 ^{+0.33} _{-0.19}	0.99	0.14	1.27	-0.1	0.0	22.06±0.02
145	J02053.0-051044.1	02:05:3.0	-05:10:44.1	1.59''	37.6 ^{+10.5} _{-9.2}	10.4 ^{+6.2} _{-4.8}	27.1 ^{+8.9} _{-7.6}	TH	0.50 ^{+0.18} _{-0.18}	3.41	0.41	4.68	0.3	0.5	20.30±0.00
146	J02052.1-050959.6	02:05:2.1	-05:09:59.6	1.57''	9.5 ^{+6.8} _{-5.5}	9.4 ^{+4.3} _{-3.5}	0.0 ^{+0.0} _{-0.0}	T	-0.69 ^{+0.09} _{-0.31}	0.84	0.36	<0.72	0.8	-0.2	26.60±0.25
147	J020446.9-051357.2	02:04:46.9	-05:13:57.2	1.67''	68.8 ^{+13.9} _{-12.6}	38.0 ^{+10.1} _{-8.8}	30.9 ^{+9.9} _{-8.6}	TSH	-0.07 ^{+0.14} _{-0.14}	7.10	1.72	5.95	-1.1	-0.2	20.07±0.01
148	J020446.8-045847.9	02:04:46.8	-04:58:47.9	1.29''	34.1 ^{+9.8} _{-8.5}	19.0 ^{+7.3} _{-6.0}	15.1 ^{+7.0} _{-5.7}	TS	-0.07 ^{+0.19} _{-0.19}	2.84	0.68	2.42	0.1	0.2	26.12±0.23
149	J020431.9-045728.1	02:04:31.9	-04:57:28.1	1.66''	47.6 ^{+12.5} _{-11.3}	20.0 ^{+8.2} _{-6.8}	27.6 ^{+9.9} _{-8.6}	TSH	0.22 ^{+0.18} _{-0.18}	4.26	0.78	4.67	0.8	-0.1	24.91±0.12
150	J020427.1-051332.7														

Table 1—Continued

ID	CXOLALA2	RA(J2000)	Dec(J2000)	Err	Tot. Cts.	Soft Cts.	Hard Cts.	det	HR	S _{0.5–10} ^e	S _{0.5–2} ^e	S _{2–10} ^e	Δα(″)	Δδ(″)	r
154	J020421.1-051038.8	02:04:21.1	-05:10:38.8	1.90″	22.4 ^{+9.1} _{-7.8}	14.9 ^{+6.7} _{-5.4}	7.4 ^{+6.5} _{-5.2}	TS	-0.32 ^{+0.35} _{-0.25}	2.17	0.63	1.36	-0.2	0.6	23.13±0.03
155	J020518.4-050720.4	02:05:18.4	-05:07:20.4	1.92″	38.1 ^{+12.0} _{-10.7}	32.0 ^{+9.7} _{-8.4}	6.1 ^{+6.6} _{-5.5}	TS	-0.66 ^{+0.22} _{-0.17}	3.56	1.31	1.08	-0.5	0.6	22.87±0.03
156	J02057.8-045859.6	02:05:7.8	-04:58:59.6	2.32″	32.4 ^{+10.8} _{-9.5}	22.5 ^{+8.3} _{-7.0}	10.0 ^{+7.4} _{-6.1}	TS	-0.34 ^{+0.26} _{-0.22}	3.84	1.16	2.24	>25.86
157	J02052.9-04578.9	02:05:2.9	-04:57:8.9	1.52″	60.8 ^{+14.5} _{-13.2}	26.7 ^{+9.5} _{-8.2}	34.2 ^{+11.3} _{-10.0}	TSH	0.19 ^{+0.17} _{-0.16}	6.98	1.34	7.38	^a
158	J020454.6-045634.3	02:04:54.6	-04:56:34.3	2.53″	30.8 ^{+12.0} _{-10.7}	12.8 ^{+8.0} _{-6.7}	18.0 ^{+9.4} _{-8.1}	TS	0.36 ^{+0.27} _{-0.33}	2.84	0.52	3.13	2.6	0.0	23.64±0.05
159	J020438.9-04597.9	02:04:38.9	-04:59:7.9	1.51″	17.7 ^{+7.9} _{-6.6}	7.6 ^{+5.4} _{-4.1}	10.2 ^{+6.2} _{-4.8}	T	0.26 ^{+0.30} _{-0.33}	1.48	0.27	1.64	>25.86
160	J020430.4-045737.6	02:04:30.4	-04:57:37.6	1.79″	64.9 ^{+13.7} _{-12.4}	34.9 ^{+9.9} _{-8.6}	29.9 ^{+9.8} _{-8.5}	TSH	-0.04 ^{+0.15} _{-0.14}	5.78	1.36	5.05	0.5	0.4	22.11±0.01
161	J020420.9-050213.7	02:04:20.9	-05:02:13.7	1.43″	17.7 ^{+7.9} _{-6.6}	12.4 ^{+6.4} _{-5.1}	5.3 ^{+5.1} _{-3.8}	TS	-0.36 ^{+0.31} _{-0.30}	1.51	0.45	0.86	0.1	-0.4	22.38±0.02
162	J020415.2-045952.7	02:04:15.2	-04:59:52.7	2.07″	18.2 ^{+10.4} _{-9.1}	1.5 ^{+9.6} _{-1.5}	16.6 ^{+9.0} _{-7.7}	T	0.82 ^{+0.18} _{-0.04}	1.71	0.06	2.95	>25.86
163	J020413.1-05062.2	02:04:13.1	-05:06:2.2	2.06″	17.5 ^{+8.8} _{-7.5}	5.5 ^{+5.3} _{-4.0}	12.0 ^{+7.3} _{-6.0}	T	0.54 ^{+0.29} _{-0.22}	1.66	0.23	2.15	1.7	0.1	23.05±0.03
164	J020411.5-05054.7	02:04:11.5	-05:05:4.7	2.02″	29.9 ^{+10.5} _{-9.3}	10.3 ^{+8.8} _{-7.5}	19.6 ^{+8.8} _{-7.5}	T	0.43 ^{+0.23} _{-0.26}	2.70	0.40	3.36	-1.3	0.4	22.23±0.02
165	J020410.5-050530.4	02:04:10.5	-05:05:30.4	2.18″	20.6 ^{+9.9} _{-8.6}	17.9 ^{+7.7} _{-6.4}	2.8 ^{+6.0} _{-2.8}	TS	-0.63 ^{+0.13} _{-0.14}	1.97	0.74	0.50	-1.4	-1.6	24.56±0.11
166	J02048.7-050353.6	02:04:8.7	-05:03:53.6	1.66″	50.3 ^{+13.2} _{-11.9}	23.6 ^{+8.5} _{-7.2}	26.6 ^{+10.5} _{-9.2}	TSH	0.12 ^{+0.18} _{-0.17}	4.67	0.96	4.65	-0.1	0.3	23.53±0.05
167	J02059.9-050836.6	02:05:9.9	-05:08:36.6	1.63″	20.5 ^{+9.0} _{-7.7}	14.7 ^{+6.9} _{-5.5}	5.8 ^{+5.9} _{-4.8}	TS	-0.40 ^{+0.35} _{-0.27}	1.71	0.53	0.92	>25.86
168	J02053.6-050925.2	02:05:3.6	-05:09:25.2	1.47″	14.5 ^{+7.3} _{-6.0}	0.0 ^{+2.3} _{-0.0}	16.1 ^{+7.2} _{-5.2}	TH	0.95 ^{+0.05} _{-0.07}	1.19	<0.07	2.52	-1.3	0.2	20.27±0.00
169	J020454.8-04545.6	02:04:54.8	-04:54:5.6	2.59″	50.7 ^{+15.6} _{-14.4}	25.2 ^{+9.9} _{-8.6}	25.5 ^{+12.5} _{-11.2}	TSH	0.07 ^{+0.24} _{-0.20}	5.39	1.21	4.98	-1.7	-0.1	21.71±0.01 ^c
170	J020449.3-045439.6	02:04:49.3	-04:54:39.6	2.22″	61.9 ^{+15.6} _{-14.4}	40.7 ^{+11.5} _{-10.2}	21.2 ^{+11.0} _{-9.7}	TS	-0.26 ^{+0.20} _{-0.18}	5.97	1.75	3.79	>25.86
171	J020443.9-045627.2	02:04:43.9	-04:56:27.2	1.74″	38.3 ^{+11.7} _{-10.4}	23.8 ^{+8.8} _{-7.5}	14.5 ^{+8.2} _{-6.8}	TS	-0.18 ^{+0.22} _{-0.21}	3.47	0.94	2.48	0.2	0.0	19.93±0.00
172	J020412.6-050458.7	02:04:12.6	-05:04:58.7	1.56″	25.8 ^{+10.2} _{-8.9}	13.4 ^{+6.7} _{-5.4}	12.4 ^{+8.1} _{-6.8}	T	0.04 ^{+0.31} _{-0.25}	2.32	0.52	2.11	-0.7	-0.3	23.77±0.02 ^d
173	J02045.5-050239.6	02:04:5.5	-05:02:39.6	2.35″	35.3 ^{+12.9} _{-11.6}	13.8 ^{+7.9} _{-6.6}	21.5 ^{+10.5} _{-9.3}	TSH	0.34 ^{+0.25} _{-0.27}	3.43	0.59	3.88	1.4	-1.8	23.69±0.06
174	J020359.4-050156.9	02:03:59.4	-05:01:56.9	4.80″	1.2 ^{+7.7} _{-1.2}	3.1 ^{+4.7} _{-3.1}	0.0 ^{+5.5} _{-0.0}	T	-0.17 ^{+0.03} _{-0.83}	0.31	0.37	<0.84	-1.8	0.9	22.94±0.06
175	J020446.8-050635.1	02:04:46.8	-05:06:35.1	0.00″	5.2 ^{+4.2} _{-2.9}	2.7 ^{+3.2} _{-1.9}	2.5 ^{+3.2} _{-1.9}	S	-0.01 ^{+0.48} _{-0.48}	0.40	0.09	0.37	0.4	0.0	26.52±0.29
176	J020451.5-050850.8	02:04:51.5	-05:08:50.8	0.99″	6.7 ^{+5.0} _{-3.6}	5.3 ^{+4.2} _{-2.9}	1.4 ^{+1.4} _{-1.4}	S	-0.52 ^{+0.16} _{-0.48}	0.53	0.18	0.22	>25.86
177	J02054.0-050930.8	02:05:4.0	-05:09:30.8	1.53″	14.8 ^{+7.5} _{-6.1}	11.6 ^{+6.2} _{-4.8}	3.1 ^{+4.2} _{-3.0}	S	-0.54 ^{+0.23} _{-0.30}	1.22	0.41	0.49	-1.1	-0.4	19.41±0.00
178	J020447.3-051239.3	02:04:47.3	-05:12:39.3	1.57″	14.6 ^{+8.1} _{-6.8}	7.1 ^{+5.6} _{-4.3}	7.4 ^{+6.2} _{-5.0}	S	0.15 ^{+0.43} _{-0.41}	1.26	0.27	1.21	-0.2	0.2	18.14±0.00
179	J020519.7-050320.9	02:05:19.7	-05:03:20.9	2.50″	34.8 ^{+12.0} _{-10.8}	18.6 ^{+8.4} _{-7.1}	16.2 ^{+9.0} _{-7.7}	S	0.04 ^{+0.26} _{-0.24}	3.05	0.71	2.68	-0.2	-0.3	23.39±0.05
180	J02051.3-045753.8	02:05:1.3	-04:57:53.8	2.42″	3.6 ^{+7.1} _{-3.6}	3.4 ^{+4.9} _{-3.4}	0.2 ^{+6.5} _{-0.2}	S	0.01 ^{+0.40} _{-0.08}	0.32	0.13	0.03	-0.4	1.4	23.75±0.07 ^c
181	J020444.2-045924.2	02:04:44.2	-04:59:24.2	1.76″	9.9 ^{+6.5} _{-5.2}	7.9 ^{+5.2} _{-3.9}	1.9 ^{+4.1} _{-1.9}	S	-0.51 ^{+0.17} _{-0.26}	0.81	0.28	0.31	-0.4	1.4	26.35±0.28
182	J020441.1-051117.4	02:04:41.1	-05:11:17.4	1.62″	13.3 ^{+7.2} _{-5.8}	12.6 ^{+6.0} _{-4.7}	0.7 ^{+4.6} _{-0.7}	S	-0.75 ^{+0.08} _{-0.25}	1.21	0.49	0.12	0.5	-1.4	24.63±0.12
183	J020419.1-050215.9	02:04:19.1	-05:02:15.9	1.72″	18.6 ^{+7.2} _{-5.8}	13.0 ^{+5.2} _{-4.7}	5.7 ^{+5.7} _{-4.5}	S	-0.34 ^{+0.36} _{-0.29}	1.70	0.51	0.99	1.2	-0.4	19.29±0.00
184	J020452.9-045556.2	02:04:52.9	-04:55:56.2	3.25″	22.4 ^{+11.7} _{-10.4}	16.4 ^{+8.4} _{-7.1}	6.0 ^{+7.2} _{-5.8}	S	-0.35 ^{+0.40} _{-0.32}	2.08	0.67	1.04	-1.7	-0.1	25.46±0.16
185	J020448.4-051018.4	02:04:48.4	-05:10:18.4	1.28″	7.6 ^{+5.8} _{-4.5}	8.7 ^{+5.4} _{-4.1}	0.0 ^{+0.0} _{-0.0}	S	-0.83 ^{+0.01} _{-0.17}	0.64	0.31	<0.42	0.4	-0.3	17.11±0.00
186	J020416.6-05033.2	02:04:16.6	-05:03:3.2	2.25″	12.6 ^{+8.1} _{-6.8}	11.6 ^{+6.5} _{-5.2}	1.0 ^{+5.4} _{-1.0}	S	-0.61 ^{+0.13} _{-0.39}	1.10	0.43	0.18	-0.6	0.6	25.05±0.16
187	J020421.9-050826.4	02:04:21.9	-05:08:26.4	1.56″	11.8 ^{+6.5} _{-5.2}	11.7 ^{+6.0} _{-4.7}	0.1 ^{+3.6} _{-0.1}	S	-0.83 ^{+0.04} _{-0.17}	2.04	0.87	0.03	0.2	1.2	16.85±0.00
188	J020448.3-050941.6	02:04:48.3	-05:09:41.6	0.84″	10.6 ^{+6.0} _{-4.7}	0.0 ^{+2.6} _{-0.0}	10.7 ^{+5.8} _{-4.5}	H	0.90 ^{+0.10} _{-0.01}	0.87	<0.08	1.69	>25.86

^aSources with the searching circles seriously overlapped by nearby bright sources and no optical counterparts can be visually identified. Reliable upper limits on their r' band magnitudes are thus not available

^bTwo Sources which are not covered by the MMT r' band image

^cSources with two counterparts identified within the searching circles. Here we only present the one which is closer to the center of the circles.

^dSources with optical counterparts visually identified. SExtractor failed to detect these counterparts due to dilution of nearby bright sources. For these counterparts, their r' band magnitudes are measured within a $1.5''$ radius circle.

^ein unit of 10^{-15} erg cm^{-2} s^{-1} .